Diurnal variability of atmospheric O_2, CO_2 and their exchange ratio above a boreal forest in southern Finland

Kim A.P. Faassen[1], Linh N.T. Nguyen[2], Eadin R. Broekema[2], Bert A.M. Kers[2], Ivan Mammarella[3], Timo Vesala[3,4], Penelope A. Pickers[5], Andrew C. Manning[5], Jordi Vilà-Guerau de Arellano[1,6], Harro A.J. Meijer[2], Wouter Peters[1,2], and Ingrid T. Luijkx[1]

[1]Meteorology and Air Quality, Wageningen University and Research, Wageningen, the Netherlands
[2]Centre for Isotope Research (CIO), Energy and Sustainability Research Institute Groningen, University of Groningen, Groningen, the Netherlands
[3]Institute for Atmospheric and Earth System Research (INAR) / Physics, Faculty of Science, University of Helsinki, Helsinki, Finland
[4]INAR/Forest Sciences, Faculty of Agriculture and Forestry, University of Helsinki, Helsinki, Finland
[5]Centre for Ocean and Atmospheric Sciences, School of Environmental Sciences, University of East Anglia, Norwich, NR4 7TJ, United Kingdom
[6]Atmospheric Chemistry Department, Max Planck Institute for Chemistry, 55128 Mainz, Germany

Correspondence: Kim A.P. Faassen (kim.faassen@wur.nl)

Abstract. The exchange ratio (ER) between atmospheric O_2 and CO_2 is a useful tracer of better understanding the carbon budget on global and local scale. The variability of ER (in mol O_2 per mol CO_2) between terrestrial ecosystems is not well-known, and there is no consensus on how to derive the ER signal of an ecosystem, as there are different approaches available, either based on concentration (ER_{atmos}) or flux measurements (ER_{forest}). In this study we measured atmospheric O_2 and CO_2 concentrations at two heights (23 m and 125 m) above the boreal forest in Hyytiälä, Finland. Such measurements of O_2 are unique and enable us to potentially identify which forest carbon loss and production mechanisms dominate over various hours of the day. We found that the ER_{atmos} signal at 23 m represents next to the diurnal cycle of the forest exchange also represents other factors, including entrainment of air masses before midday, with different thermodynamic and atmospheric composition characteristics in the atmospheric boundary layer. To derive ER_{forest} we infer O_2 fluxes using multiple theoretical and observation-based micro-meteorological formulations to determine the most suitable approach. Our resulting ER_{forest} shows a distinct difference in behaviour between daytime (0.92 ± 0.17 mol/mol) and nighttime (1.03 ± 0.05 mol/mol). These insights demonstrate the diurnal variability of different ER signals above a boreal forest and we also confirmed that the signals of ER_{atmos} and ER_{forest} can not be used interchangeably. Therefore, we recommend measurements on multiple vertical levels to derive O_2 and CO_2 fluxes for the ER_{forest} signal, instead of a single level time series of the concentrations for the ER_{atmos} signal. We show that ER_{forest} can be further split into specific signals for respiration (1.03 ± 0.05 mol/mol) and photosynthesis (0.96 ± 0.12 mol/mol). This estimation allows us to separate the Net Ecosystem Exchange (NEE) into Gross Primary Production (GPP) and Total Ecosystem Respiration (TER), giving comparable results to the more commonly used eddy covariance approach. Our study shows the potential of using atmospheric O_2 as an alternative and complementary method to gain new insights into the different CO_2 signals that contribute to the forest carbon budget.

1 Introduction

To understand how the increasing carbon dioxide (CO_2) levels in the atmosphere are will change our climate, we need to know the sources and sinks of CO_2 separately. The main sources are fossil fuel combustion and land-use change and the main sinks are the net uptake by the terrestrial biosphere and the oceans (Friedlingstein et al., 2022). The net terrestrial biospheric sink (Net Ecosystem Exchange, NEE) results from many fluxes of which the two largest are typically Gross Primary Production (GPP) and the Total Ecosystem Respiration (TER). Knowing these gross fluxes separately will allow better estimates of the changing behaviour of the biosphere carbon sink, as GPP and TER respond differently to climate change and increasing atmospheric CO_2 levels (Cox et al., 2013; Ballantyne et al., 2012).

Using tracers in addition to CO_2 allows us to gain further insights into GPP and TER, without relying on a temperature-based function to parameterize TER as is used for Eddy Covariance (EC) measurements (e.g. Reichstein et al. (2005)). Tracers such as atmospheric O_2 (Keeling and Manning, 2014), and also COS, $\delta^{13}C$ or $\Delta^{17}O$ have the important advantage of sharing a process or pathway with CO_2 directly (Wehr et al., 2016; Whelan et al., 2018; Peters et al., 2018; Koren et al., 2019; Kooijmans et al., 2021). This allows one to use numerical models to test formulations of processes, such as stomatal and mesophyl exchange, photosynthesis, pool-specific respiration, and even turbulent canopy exchange. Atmospheric O_2 is directly coupled to CO_2 in several processes through the so-called Exchange Ratio (ER) (Keeling and Manning, 2014; Manning and Keeling, 2006; Keeling et al., 1993). This ER indicates the number of moles of O_2 that are consumed per moles of CO_2 that are produced (or vice versa) and gives a process-specific signature (Keeling, 1988).

On the global scale, the O_2:CO_2 molar ratio ER has been used to derive the global oceanic CO_2 sink and determine the global carbon budget (Stephens et al., 1998; Rödenbeck et al., 2008; Tohjima et al., 2019). This is done by solving the atmospheric budgets of O_2 and CO_2 with the following equations:

$$\frac{dCO_2}{dt} = F - O - B \tag{1}$$

$$\frac{dO_2}{dt} = -\alpha_F F + \alpha_B B + Z_{O_2} \tag{2}$$

where F is the fossil fuel CO_2 emissions, O is ocean CO_2 uptake, B is the net terrestrial biosphere sink of CO_2 and Z_{O_2} indicates the ocean O_2 outgassing. α_F and α_B indicate the global ERs for fossil fuel combustion and the net terrestrial biosphere sink respectively. In these global studies simplified global average values ares used for α_F and α_B, where α_F is determined from the global mixture of fuels burned, which results in 1.38 [mol/mol] (Keeling and Manning, 2014) and α_B was determined by laboratory measurements and a literature study of different plant and soil materials, which resulted in 1.1 [mol/mol] (Severinghaus, 1995). Furthermore, α_B is used to combine O_2 and CO_2 into Atmospheric Potential Oxygen (APO) (Stephens et al., 1998) which is used in determining the ocean carbon sink, and recently has also been shown to be a suitable tracer to detect fossil fuel emission reductions during the COVID-19 pandemic (Pickers et al., 2022). For these larger scale applications using

APO it is important to have good estimates for the terrestrial biosphere ERs.

On local/ecosystem scales previous studies have shown that this terrestrial biosphere ER is not a constant value of 1.1 as used on the global scale, and that is shows a certain degree of temporal and spatial variability. These studies either measured the Oxidative Ratios (ORs) from elemental composition analysis (Worrall et al., 2013; Randerson et al., 2006; Gallagher et al., 2017), or derived the ER from atmospheric concentrations measurements (Battle et al., 2019; Seibt et al., 2004; van der Laan et al., 2014). Note that there is a distinction in the terminology between ER and OR. The OR indicates the stoichiometry of specific materials, whereas the ER indicates the exchange between the atmosphere and organisms or ecosystems. By using elemental composition analysis, the OR reflects the relationship between O_2 and CO_2 over a longer time scale, of years or decades and only reflects the OR from the materials that are sampled. By using atmospheric concentration measurements for the ER, the ER reflects a shorter time scale compared to the OR, of hourly to daily time periods and it also reflects a different spatial scale, as the ER includes all processes that are originating from the footprint. The spatial scale that is covered by the ER signal depends on the type of measurements or modelling, i.e. leaf, canopy or ecosystem. Both the OR and the ER based studies showed that O_2:CO_2 molar ratio of the biosphere changes per ecosystem and over different time periods. The ER from the gas exchange experiments can furthermore be used for the separation of GPP and TER, using a specific ecosystem ER, which are determined with two alternative approaches (see Figure 1) (Seibt et al., 2004; Stephens et al., 2007; Ishidoya et al., 2013, 2015; Battle et al., 2019). The first is the ER of the atmosphere (ER_{atmos}), which is the ratio of the evolution of the atmospheric O_2 and CO_2 concentration measurements over time, and the second is the ER of the forest (ER_{forest}), which is the ratio of the net surface fluxes of O_2 and CO_2 above the canopy, including all processes occurring below the canopy, including both vegetation and soil exchange. First attempts to estimate ER_{forest} were made using one-box models (Seibt et al., 2004; Ishidoya et al., 2013). More accurate estimates of ER_{forest} would be based on in-situ measured O_2 and CO_2 surface fluxes, however O_2 currently cannot yet be measured accurately using EC techniques. Ishidoya et al. (2015) showed the first surface fluxes of O_2 using vertical gradients of O_2, an alternative technique to EC, and CO_2 measurements at two heights above the canopy in the surface layer in a temperate forest in Japan. Their results showed that the ER_{forest} signal could be used to separate the NEE signal into GPP and TER, consistent with the separation method for EC measurements using an empirical function of air temperature.

When using O_2 to separately estimate GPP and TER fluxes, it is important to use the value for ER that represents ecosystem exchange. Seibt et al. (2004) showed that the signal of ER_{atmos} cannot be directly linked to the exchange of carbon in the terrestrial biosphere, because in addition to the biosphere, ER_{atmos} is also affected by advection, boundary layer dynamics and entrainment (Figure 1). In contrast, Ishidoya et al. (2015) found similar values for ER_{atmos} and ER_{forest}. So far, there is no clear consensus on which signal should be used to indicate the ER of the ecosystem. Furthermore, since atmospheric O_2 measurements are challenging to make, only a few studies exist that measured atmospheric O_2 from flasks (Seibt et al., 2004) or continuously (Ishidoya et al., 2015; Stephens et al., 2007; Battle et al., 2019) above an ecosystem and derive ER signals. The uncertainty and spatial and temporal variability of O_2:CO_2 molar ratio of the biosphere are therefore not well known

(Manning and Keeling, 2006; Keeling and Manning, 2014), and knowledge about the difference between ER_{forest} and ER_{atmos}, its variability across difference regions and ecosystems, and how ER_{forest} can be used on both the local and global scale to advance our understanding of the carbon cycle, is still limited. Therefore, more and longer in-situ time series of atmospheric
90 O_2 measurements are needed and further understanding of O_2 and CO_2 exchange above and below the canopy is crucial to continue the pioneering work of Seibt et al. (2004), Stephens et al. (2007), Ishidoya et al. (2015) and Battle et al. (2019) and improve the application of the global biosphere ER, resulting in a better understanding of the carbon balance on local, regional and global scales.
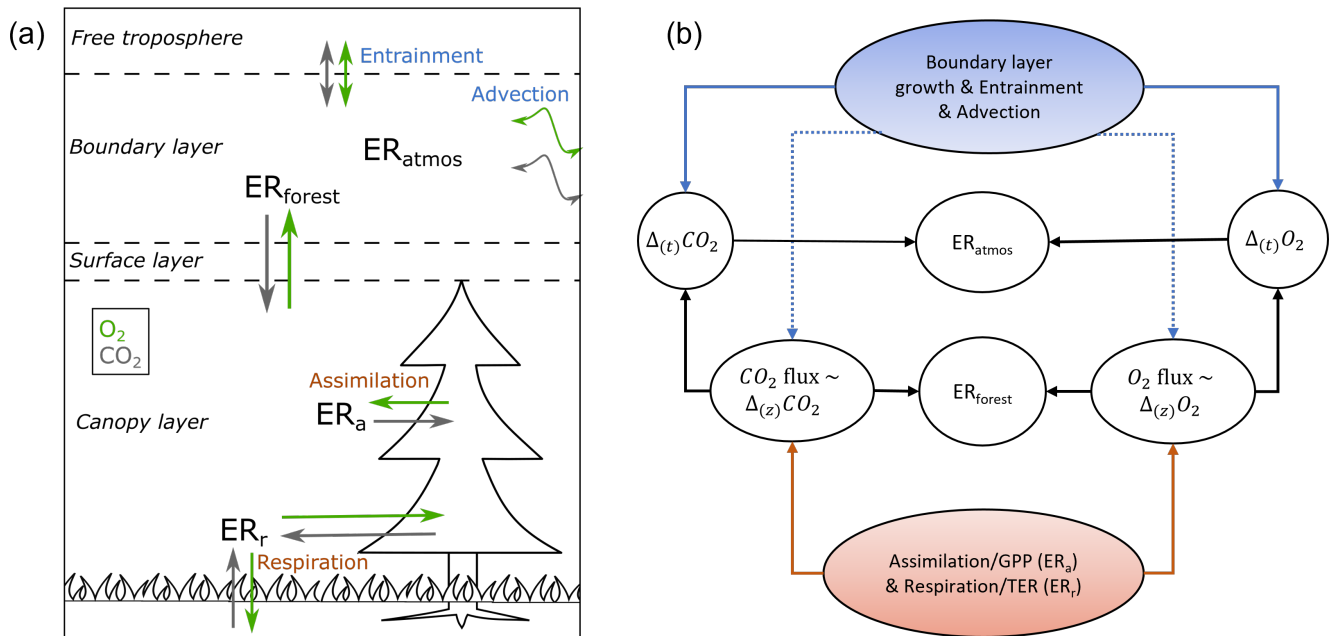
Figure 1. Schematic overview of the different O_2:CO_2 exchange ratio signals (ER), measured and analyzed in and above a forest, influenced by the different O_2 and CO_2 fluxes and meteorological processes (a), together with a more detailed look on which processes influence the different ER signals (b). (a) shows the direction of the surface fluxes during the day in the surface layer, which includes the roughness sublayer and the inertial sublayer. During the night the direction of the O_2 and the CO_2 surface fluxes are the other way around. The ER of the atmosphere (ER_{atmos}) is determined from the change over time ($\Delta_{(t)}$) in the O_2 and CO_2 concentration measurements, and the ER of the forest (ER_{forest}) is calculated from the surface fluxes of O_2 and CO_2 which are inferred from ($\sim$) the vertical gradient ($\Delta_{(z)}$). ER_a represents assimilation processes that influence the Gross Primary Production (GPP) flux and ER_r represents respiration processes that influence the Total Ecosystem Respiration (TER) flux. (b) shows the connections between the processes, measurements, and the ERs. Dotted lines indicates smaller influences of the processes that are connected to it compared to solid lines.

95   The aim of this study is to improve upon existing methods to calculate ER_{forest} and get a better comparison of the ER_{atmos} and ER_{forest} signals. We carried out a measurement campaign in Hyytiälä, Finland, for two short periods in spring/summer

2018 and 2019 where both O_2 and CO_2 were measured at two heights with a setup including a differential fuel cell analyser for O_2. We used our measurements to determine the diurnal behaviour of the relation between the concentrations and the fluxes of O_2 and CO_2, by using either one or both measurement heights on the tower. The objectives of this study are: 1) to extend the existing continuous O_2 records, 2) to calculate the O_2 surface fluxes in a boreal forest for the first time, 3) to combine the O_2 and the CO_2 fluxes, to calculate ER_{forest} from these fluxes, and to compare the ER_{atmos} and ER_{forest} signals, and 4) use ER_{forest} to estimate GPP and TER fluxes.

In this paper, we first describe the measurement site, experimental setup and methods used to derive O_2 fluxes and the different ER signals (Section 2). We present the measurements for the whole campaign and select a representative day to determine the most suitable approach for deriving O_2 fluxes and to determine ER_{forest} (Section 3). A detailed evaluation and discussion of our ER_{atmos} and ER_{forest} signals is given in Section 4. We finalize with our conclusion about the diurnal variability of the ER signals for a representative day of a boreal forest (Section 5).

2   Methods

To determine ER_{atmos} and ER_{forest}, and its diurnal variability, we measured O_2 and CO_2 continuously at two heights above a boreal forest during two short campaigns at Hyytiälä. These 'OXHYYGEN' (OXYGEN at HYYtiälä) campaigns took place in the spring/summer of 2018 (03-Jun through 02-Aug) and 2019 (10-Jun through 17-Jul). In this section, we describe the measurement site and instrumental setup, as well as the methods used to determine the O_2 and CO_2 fluxes from the measured vertical gradient and the ER signals.

2.1   Measurement site

The measurements were made at Hyytiälä SMEAR II Forestry Station of the University of Helsinki in Finland (61° 51'N, 24°17' E, +181 MSL); this site is described in more detail in e.g. Hari et al. (2013). The SMEAR II station is a boreal site within the European Integrated Carbon Observation System (ICOS) network with atmospheric and ecosystem measurements. The SMEAR II station is located inside a homogeneous forest of Scots pine trees (*Pinus Sylvestris*) with a dominant canopy height of 18 m and some silver birch and aspen trees. The forest floor is covered with mosses and herbs. The soils are podzols on top of glacial till. A large lake is located close (around 550 m) to the measurement site and has a fetch of 250 m over the dominant wind direction of 230°. The footprint of the site is mostly influenced by natural sources, with the atmospheric signal dominated by forest exchange (Carbon Portal ICOS RI, 2022). The measurement site includes several towers, including a 128m tall tower and a 23 m high walk up tower, where atmospheric variables and gas concentrations are continuously measured. The operational data from this tower are publicly available online at http://avaa.tdata.fi/web/smart/smear/. Our O_2 and CO_2 measurement setup was installed in a cabin at the bottom of the 23 m high tower, and air was sampled from aspirated inlets (Blaine et al., 2006), installed at 23 m in the smaller tower and at 125 m in the tall tower, 5m and 107m above the canopy

height respectively. We used both levels to calculate the vertical gradient for the flux calculations (Section 2.3).

2.2 Experimental setup

The measurement setup is based on the instrument used in van Leeuwen and Meijer (2015), following the methods in van der Laan-Luijkx et al. (2010) and Stephens et al. (2007). O_2 is measured with a Sable Systems "Oxzilla II" fuel cell based instrument and CO_2 is measured with an ABB continuous gas analyzer "URAS26", which is a non-dispersive infrared (NDIR) photometer. The gas handling schematic is shown in Figure 2.
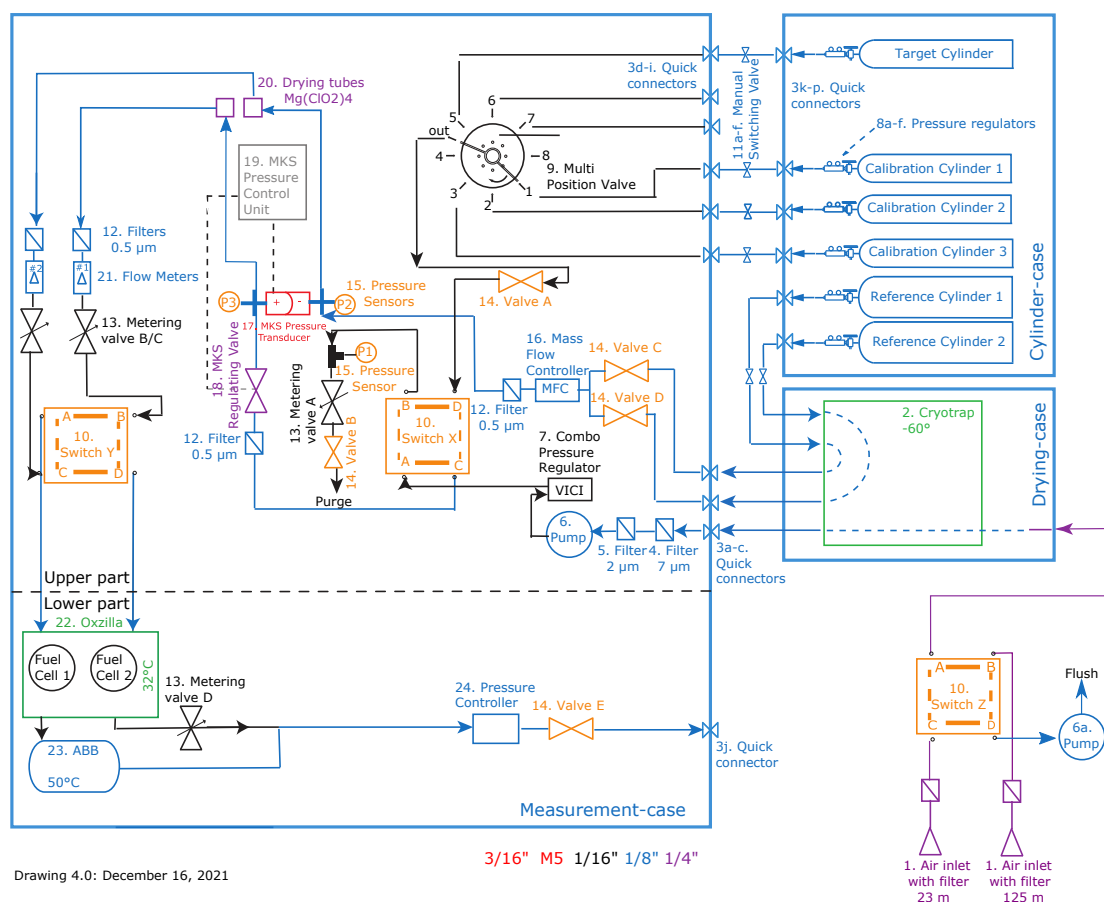
Figure 2. Schematic overview of the measurement setup used at Hyytiälä. The setup includes an Oxzilla O_2 fuel cell analyser and a URAS26 NDIR CO_2 analyser. The system measured air sampled from two heights of either 23 or 125 meters.

Air was pumped from either 23 or 125 metre height to the measurement system at the base of the tower. Both inlet lines were continuously flushed, where either one of the heights is measured by the system with a sample flow of around 120 ml/min and the other flushed to the room with a higher flow rate of around 2 litre per minute, which allows fast switching between the two heights. We switched between the inlets every half hour to match the EC measurements of ICOS that were already present in the tower and to get a more stable signal of O_2. The air of the selected inlet was first cooled to -60 °C with a cryogenic cooler to remove water vapour from the air, before entering the system. Second stage drying of the air streams was done with magnesium perchlorate $(Mg(ClO_4)_2)$ traps. The sample air was continuously measured against a reference gas (differentially for O_2, and alternatively for CO_2), and the pressure in both sample and reference line were matched to be the same using a pressure control system (MKS Instruments, types 223B, 248A and 250E for the pressure transducers, regulating valve and control system respectively). The reference and sample lines were switched every 2 minutes between the two fuel cells in the Oxzilla analyser. We measured a set of 3 calibration cylinders and 1 target cylinder every 23 hours for half an hour per cylinder.

The measurements of these calibration gases allowed calibration of our measurements against the international Scripps Institution of Oceanography (SIO) scale for $\delta O_2/N_2$. We did that by using cylinders that are filled in the laboratory at the University of Groningen, where they were calibrated with the primary Scripps cylinders (Nguyen et al., 2022). The O_2 measurements are normally expressed as $\delta O_2/N_2$ ratios in 'per meg' units instead of mole fraction (ppm), since O_2 is not a trace gas because of its high abundance of 20.95%, and therefore the mole fraction varies due to changes of other gases, such as CO_2 (Keeling et al., 1998). $\delta O_2/N_2$ is defined as:

$$\delta(O_2/N_2) = \left(\frac{(O_2/N_2)_{\text{sample}}}{(O_2/N_2)_{\text{reference}}} - 1 \right) \cdot 10^6 \text{ [per meg]} \tag{3}$$

For simplicity, in this paper we use the term O_2 instead of $\delta O_2/N_2$, and we use the term 'concentration' rather than 'mole fraction' when discussing both CO_2 and O_2. Equation 3 indicates a change compared to a reference level. Negative values therefore indicate concentrations of O_2 lower than the reference value. To allow comparison of changes in CO_2 and O_2 directly, we converted the units of O_2 from per meg to ppm equivalents (ppmEq), where a change of 1 ppm CO_2 corresponds to a 4.77 per meg change in O_2 (Tohjima et al., 2005; Kozlova and Manning, 2009).

We modified the method described in van der Laan-Luijkx et al. (2010), to calibrate the measurements. The raw CO_2 measurements have a frequency of one measurement per six second, the raw O_2 measurements have a frequency of one measurement per second and both give 1 value every 4 minutes in the form of ΔCO_2 and $\Delta(\Delta)O_2$ respectively. CO_2 is measured on a single cell instrument, and therefore ΔCO_2 is the difference between the 2-minute averages of the sample air (S) and the reference cylinder (R), giving (S-R). For the 2-minute averaged CO_2 measurements, the last 78 seconds of each 2 minute period are used. Note that for CO_2, the NDIR system is different compared to other systems used and therefore does not need a zero-gas (Pickers et al., 2017). O_2 is measured on a double cell instrument, and therefore gives a double differential signal. The $\Delta(\Delta)O_2$ is the difference between the 2-minute averaged difference between S and R and the 2-minute averaged difference between R and S ((S-R)-(R-S)). For the 2-minute averaged O_2 values, the last 100 seconds of each 2 minute period are used. In

2019, the MKS pressure control valve was not functioning optimally, and led to a small instability in the differential pressure between the sample and reference lines. We therefore corrected the 4-minute values of $\Delta(\Delta)O_2$ for this deviation measured by the MKS differential pressure sensor (PMKS), by multiplying $\Delta(\Delta)O_2$ with 0.095*PMKS, which we derived based on the measurements of the calibration cylinders. In 2018, there was no instability in the pressure control valve, and therefore no correction was applied in that year. The PMKS deviations correlated with temperature and increased towards the end of the 2019 campaign. Figure B1 in Appendix B shows that the highest corrections were made during the mid-day at the end of the campaign. The O_2 vertical gradient is hardly affected by the correction as it is the difference between measurements at two heights which are both undergoing the same deviation.

For both CO_2 and O_2, the 4-minute values were subsequently used to calculate half hourly means, where we excluded the first 4-minute value after the heights are switched, together with the measurements that did not fall inside the boundary based on the median absolute deviation (MAD) (Rousseeuw and Verboven, 2002). For every half hourly mean, a standard error is calculated (see equation 4) which is used in further analysis to determine the uncertainty of our measurements.

The linear calibration response functions for both O_2 and CO_2 were calculated for every measurement period of the calibration cylinders, which was about every 23 hours. For the response functions, we used a constant slope based on the mean of all the calibration slopes measured in the specific year. The y-intercept of the response functions were interpolated to the time of the measurement, based on the two calibrations bracketing the measurement time. To facilitate the comparison of the O_2 and CO_2 measurements of the two heights and allow flux calculations based on the vertical gradient, we interpolated the data to one measurement for every 30 minutes for each height. Based on the target cylinders, measured during the calibration period, the stability of the long-term measurements were determined (Table 1). A different target cylinder, with different composition of air for 2019 compared to 2018 was used, which resulted in different outcomes for the standard deviation (std) and the mean difference for these periods. The mean difference is calculated from the target measurements at Hyytiälä compared to the calibrated values using the SIO cylinders in Groningen. The measurement period of 2018 was also longer and therefore more points were included for the std and mean difference calculations. The long-term measurement precision of this device throughout the duration of the two measurement campaigns compared to the recommendations of the World Meteorological Organisation (WMO) will be further discussed in section 4.1.

Table 1. The mean difference and the standard deviation (std) of the target cylinder measurements of O_2 and CO_2 for the 2018 and 2019 periods separately, together with the number of data points used to calculate these specific values.

	2018 (03-06 through 01-08)			**2019** (16-06 through 17-07)		
	Std	Mean difference	Number of points	Std	Mean difference	Number of points
O_2 [per meg]	16	28	53	19	22	22
CO_2 [ppm]	0.07	0.7	53	0.07	0.5	22

2.3 Data analysis

For the analyses presented in this paper we needed representative diurnal cycles of O_2 and CO_2. We looked for a representative day in 2019 where little to no clouds were present, no unexpected behaviour in the diurnal cycles for potential temperature, specific humidity and CO_2 occurred, (for example caused by advection) and where the O_2 data showed a clear difference between the two measurement heights. We used data from 2019 instead of 2018 because 2018 saw a large-scale drought in Europe, and 2019 was less extreme and closer to a typical boreal summer (Peters et al., 2020). However, no single representative day could be found in our 2019 record, where the O_2 data showed a clear negative vertical gradient during the day and positive during the night, in combination with the above-mentioned meteorological criteria. We therefore choose a sequence of days to create an aggregate day based on the average of several days, which is representative for this time of the year in Hyytiälä, following the same method used by Ishidoya et al. (2015). The main criterion was that the vertical O_2 gradient had to be negative during the day and the negative relationship between the change of O_2 and CO_2 concentrations over time at 23 m was present during the entire day. This resulted in selecting the period of 7 through 12 July 2019 to create the representative day which we used in all subsequent analyses. The half-hourly values for the representative day are the averages of the data points of the individual half hourly values for each day in the selected period. Each time step has an uncertainty which is based on the error propagation of the standard error (SE) of the 30-minute averages for each day in the aggregate and is calculated for each time step with:

$$SE_{aggr} = \frac{\sqrt{\sum SE_{day}^2}}{n} \tag{4}$$

Where n is the number of days included in the aggregate, SE_{day} is the Standard Error of the 30-minute average of each individual day and the SE_{aggr} is the resulting Standard Error of a 30-minute value for the representative aggregate day.

For the representative day, the two $O_2 : CO_2$ Exchange Ratio (ER) signals, ER_{atmos} and ER_{forest}, were determined. ER_{atmos} is concentration-based and is expressed as:

$$ER_{atmos} = -\frac{\Delta_{(t)}O_2}{\Delta_{(t)}CO_2} \tag{5}$$

Where both $\Delta_{(t)}O_2$ and $\Delta_{(t)}CO_2$ are the change in concentration over a selected time period (t). This is a unit-less quantity as it represents mol O_2 per mol CO_2. ER_{atmos} was determined by the slope of a linear regression between the concentration of O_2 and CO_2 at the same height over a specific time period (Seibt et al., 2004; Stephens et al., 2007; Ishidoya et al., 2013; Battle et al., 2019). The selected time periods were based on the period when O_2 and CO_2 had the highest negative correlation. Throughout the day, this could be divided into three periods when different processes dominate (Figure 1). It starts with the period during the night where the atmosphere is stable and respiration becomes the dominant surface flux (P1), and therefore the CO_2 concentration increases and the O_2 concentration decreases. Subsequently, when the sun starts to rise, the boundary layer height starts to grow and entrainment of air from the free troposphere influences the surface measurements (P2) (Vilà-Guerau de Arellano et al., 2004). Here the CO_2 concentration decreases rapidly and the O_2 concentration increases rapidly. Finally,

the period starts when the effect of boundary layer dynamics and entrainment decreases and the assimilation flux dominates
(P3), here the CO_2 concentration decreases less rapidly and the O_2 concentration increases less rapidly. We calculated a ER_{atmos}
signal with equation 5, for the night-time (P1), the day-time (by either focusing on only P3 or both P2 and P3) and the complete
day (P1 + P2 + P3). The exact boundaries of these periods have to be estimated. To be certain about the exact times that should
be taken as the boundaries for each period, an atmospheric model is needed.

ER_{forest} is flux-based and is expressed as:

$$ER_{forest} = -\frac{F_{O_2}}{F_{CO_2}} \tag{6}$$

Where both F_{O_2} and F_{CO_2} are the net mean turbulent surface fluxes above the canopy of O_2 and CO_2 over a selected time
period (Seibt et al., 2004; Ishidoya et al., 2015). We derive the fluxes of O_2 and CO_2 using the vertical gradient (see next
paragraph and Equation 7). The selected time periods for ER_{forest} were chosen such that the transition periods between the
nighttime with a stable atmosphere (when the respiration flux dominates) to the daytime with a well mixed atmosphere (when
assimilation dominates), were excluded. By excluding the transition periods, we removed the periods where the gradients of
both CO_2 and O_2 were close to zero. This was done because a very small gradient makes it difficult to calculate a flux and
therefore the ER_{forest}, and also because during this period entrainment is the most dominant process. The exact duration of the
transition periods was based on the maximum and minimum of both the friction velocity and the height of 27 m (z) divided
by the Monin Obukov Length (L). The friction velocity and (z/L) indicate the measure of turbulence of the atmosphere (Stull,
1988). The mean of the remaining data points of the CO_2 and O_2 flux during the stable atmosphere period was used to calculate
the ER_{forest} signal of the night and the mean of the remaining data points of the CO_2 and O_2 flux during the mixed atmosphere
period was used to calculate the ER_{forest} signal of the day. The ER_{forest} for the entire day is taken as the average CO_2 and O_2 flux
over the entire day. For this average no periods are excluded and all the data points over the 24 hours are taken into account.
Taking the average daily fluxes to derive ER_{forest} is a slightly different approach compared to the study of Ishidoya et al. (2015),
who use the regression line between $\Delta_{(z)}O_2$ and $\Delta_{(z)}CO_2$ to determine ER_{forest}.

Currently, unlike for CO_2, the O_2 flux cannot be measured directly with an EC system. Instead, the flux can be inferred from
the flux-gradient method. To calculate the flux of a certain scalar (ϕ) with the flux-gradient method, the following equation was
used (Stull, 1988):

$$F_\phi = -K_\phi \cdot \frac{\partial \overline{\phi}}{\partial z} \tag{7}$$

Where F_ϕ is the surface flux of ϕ, K is the exchange coefficient and $(\partial \overline{\phi}/\partial z)$ is the vertical gradient of $\overline{\phi}$. To determine the O_2
flux with Equation 7 ($\overline{\phi} = \overline{O_2}$), the exchange coefficient of O_2 (K_{O_2}) needs to be determined. Ishidoya et al. (2015) assumed
that $K_{O_2} = K_{CO_2}$ and determined K_{CO_2} by dividing the CO_2 flux, measured with EC, by the CO_2 vertical gradient between
two measurement levels. However, the exchange coefficient can also be determined with other methods that for example only
need two measurement heights for the vertical gradient. In this study, we explore these different options for calculating K_{O_2}.

The EC measurements of the CO_2 flux were used as a reference, to determine the most suitable approach. The most suitable approach to infer the O_2 flux is then used for both K_{CO_2} and K_{O_2}. During this study we derive the surface flux in the surface layer (Figure 1) and we assume that the surface flux stays constant in this surface layer, which consists of the roughness sub-layer and the inertial sublayer.

We categorized the methods to determine the most suitable K into two groups: The observation-based approach (also called the K-theory (Stull, 1988) or the modified Bowen ratio method (Meyers et al., 1996)) and the theoretical approach (following the similarity theory (Dyer, 1974)). For the observation-based methods, we determined the exchange coefficient (K) in equation 7 by dividing a flux measured at 27 m, using an EC system, by a 3-height (16 m, 67 m and 125 m) vertical gradient of a specific scalar. Ishidoya et al. (2015) used this approach to calculate their O_2 flux, using the CO_2 flux and vertical gradient of two levels. Next to CO_2, we also calculated K using potential temperature (θ) for the observation-based approach.

For the theoretical approach, the K in equation 7 is determined with the Monin-Obukov Similarity Theory (MOST) (Dyer, 1974), where logarithmic surface layer scaling applies for K and empirical similarity functions are used to describe the effect of atmospheric stability. In addition, we used a correction which takes into account the effect of the roughness sublayer (see Appendix for details). The SMEAR II data at 27 meter were used for the calculations with MOST. When only two heights for the gradient calculations are available, there is an option to integrate equation 7 (de Ridder, 2010). We tested both the application with and without integration in this study. We used the ICOS data, available at the SMEAR II station, for the K calculations. For the CO_2 EC measurements, we used the gap-filled data to correct for the storage below the measurement height of the EC. Gap-filling was applied when the friction velocity (u*) was below 0.4 m s^{-1} (Kulmala et al., 2019). The Appendix gives a more elaborate explanation and provides equations of the different methods used to determine the exchange coefficients used in this study.

Finally, we select the K_ϕ from either the observation-based or the theoretical approach that produced CO_2 flux results from our CO_2 vertical gradient measurements that showed the best comparison to the EC CO_2 flux measurements. This K was used to calculate the O_2 and CO_2 fluxes, together with the vertical gradient from measurements collected during our campaigns. For our campaigns, we only have O_2 and CO_2 measurements at two heights (23 m and 125 m), which means that $(\partial\overline{\phi}/\partial z)$ changes into $(\Delta\overline{\phi}/\Delta z)$ and the gradient was calculated with finite differences.

After both the CO_2 and O_2 fluxes were determined, resulting in ER_{forest}, we subsequently calculated the $O_2 : CO_2$ exchange ratio signals for the assimilation processes (ER_a) and the respiration of the ecosystem (ER_r) with the following equations (Seibt et al., 2004; Ishidoya et al., 2015):

$$NEE = -GPP + TER \tag{8}$$

$$NEE \cdot ER_{forest} = -GPP \cdot ER_a + TER \cdot ER_r \tag{9}$$

Where the NEE is the Net Ecosystem Exchange, GPP is the Gross Primary Production and TER is the Total Ecosystem Respiration. GPP and TER are always positive by definition, representing uptake and release by the ecosystem respectively. Therefore, when GPP is larger than TER the resulting negative NEE values represent carbon uptake by the ecosystem. First, we assumed that nighttime NEE is equal to TER, which meant that the nighttime ER_{forest} signal is equal to ER_r. We assumed that the processes that contributed to the ER_r keep the same ratio between O_2 and CO_2 during the entire day and therefore we used a constant ER_r for the entire day. We base this assumption on studies that showed that the variability of ER_r highly depends on the bulk soil respiration (Hilman et al., 2022; Angert et al., 2015). No large changes occur in the soil temperature and the soil moisture during our (representative) diurnal cycle, and therefore we assume that the ER_r of the bulk soil respiration stays relatively constant and with that the ER_r of the ecosystem also stays constant over the entire day. Subsequently, we calculated ER_a, for both the entire diurnal cycle and the daytime using equation 9 with the corresponding ER_{forest} and the constant ER_r. We used ICOS NEE EC measurements from the SMEAR II station at a level of 27 meters in the 128 m high tower. The GPP fluxes at Hyytiälä are calculated with either of the following 2 approaches: 1) when NEE EC measurements are available, GPP is calculated as the difference between the NEE EC measurements and the respiration flux, which is calculated using a temperature function or 2) when NEE EC measurements are not available, GPP is calculated using an equation that is based on the air temperature and light (Photosynthetically active radiation (PAR)). A more detailed description of these calculations is given by Kulmala et al. (2019) and Kohonen et al. (2022).

By estimating ER_r and ER_a of this boreal forest, we created the opportunity to apply atmospheric O_2 measurements to separate NEE into GPP and TER (the O_2 method). We calculated ER_r and ER_a for the representative day using equations 8 and 9, and use these to calculate GPP and TER for another representative day. We selected 13 through 15 June to create a new second aggregate day and to calculate a new ER_{forest} signal for the entire day (see figure 3 d and e) for a detailed view on the measurements of those days). These three days were chosen because in 2019 they showed the clearest diurnal cycle of O_2 and a negative O_2 gradient, aside from 7 through 12 July, used above. We assume here that the ER_r and ER_a calculated for the period from 7 through 12 July are representative for the period from 13 through 15 June. Studies show that the ER_r (Hilman et al., 2022) and ER_a (Bloom, 2015; Fischer et al., 2015) vary with changing soil and atmospheric conditions. The periods for both representative days are relatively close in time and therefore have similar conditions in the soil and the atmosphere, and we can therefore assume that the ER_r and ER_a based on the 7 through 12 July data can also be applied to the 13 through 15 June period. By using the ER_r and ER_a determined for the first representative day (7-12 July), and ER_{forest} and NEE for the second representative day (13-15 June), we calculated GPP and TER from NEE for this second representative day. By comparing the GPP and TER fluxes of the O_2 method to the GPP and TER fluxes of the temperature-based function of ICOS (EC method), we could demonstrate how accurate the O_2 method is (Section 3.4). Both Seibt et al. (2004) and Ishidoya et al. (2015) also applied the O_2 method, however both these studies used chamber measurements to first determine ER_a and ER_r and then used equation 8 and 9 to infer GPP and TER. Unfortunately we did not have chamber measurements of both O_2 and CO_2 available and therefore we used equation 8 and 9 to calculate ER_a and ER_r. This means that these two equations can be used in two

330 ways: to determine the ER_a and ER_r signal, or to separate NEE into GPP and TER.

The footprint of the calculated O_2 and CO_2 surface fluxes which also represents the footprint of the ER_{forest}, ER_r and ER_a signals for the representative aggregate day is shown in Figure B2 in Appendix B. The footprint is based on the method of Kljun et al. (2015) where for the height, the geometric mean between 125 m and 23 m is used. The footprint analysis shows
335 that the surface fluxes are mainly influenced by the forest surrounding the tower and that the lake located close to the tower is not influencing the signal. The footprint of the O_2 and CO_2 concentrations and therefore the footprint of the ER_{atmos} signal can be found in the document of (Carbon Portal ICOS RI, 2022). This concentration footprint analysis shows that with an average wind direction of north to northeast between 7 through 12 July 2019, the concentrations measured are mainly originated from forest exchange, with hardly any influence of urban sources.
340
Table B1 in Appendix B gives a complete overview of which data are used for each part of this research for the two different aggregate days.

3 Results

345 ### 3.1 O_2 and CO_2 time series

The calibrated half hourly measurements of O_2 and CO_2 for 2018 and 2019 are shown in Figure 3, together with the vertical gradients between the two measurement heights. The O_2 measurements are shown here converted from per meg to ppmEq, to allow comparison of the diurnal variability for CO_2, and to calculate the ER signals. The differences between the 23 m and 125 m measurements are observable for both CO_2 and O_2. During both campaigns in 2018 and 2019, the diurnal behaviour of
350 the O_2 concentrations are anticorrelated with the CO_2 concentrations. This anticorrelation between O_2 and CO_2 is also visible from the gradient measurements, despite the relatively high uncertainty of the O_2 measurements as described in Section 2.2 and further elaborated on in Section 4.1. The period 7 through 12 July 2019 shows the most clear negative relationship between the O_2 gradient and the CO_2 gradient, and also had the most suitable meteorological conditions and was therefore selected for the aggregate representative day (Section 2.3). The period 13 through 15 June shows a less clear anticorrelation between the
355 vertical gradients of O_2 and CO_2 (Figure 3 d and e), but with clear diurnal cycles of O_2 and CO_2 suitable for the purpose of our second aggregate day (see Section 3.4).

3.2 Diurnal cycles

The measurements of O_2 and CO_2 and their vertical gradient for the representative day, are shown in Figure 4. There are no
360 measurements between 20:00 and 22:00 because the calibration cylinders were measured during this period. For 7 through 12
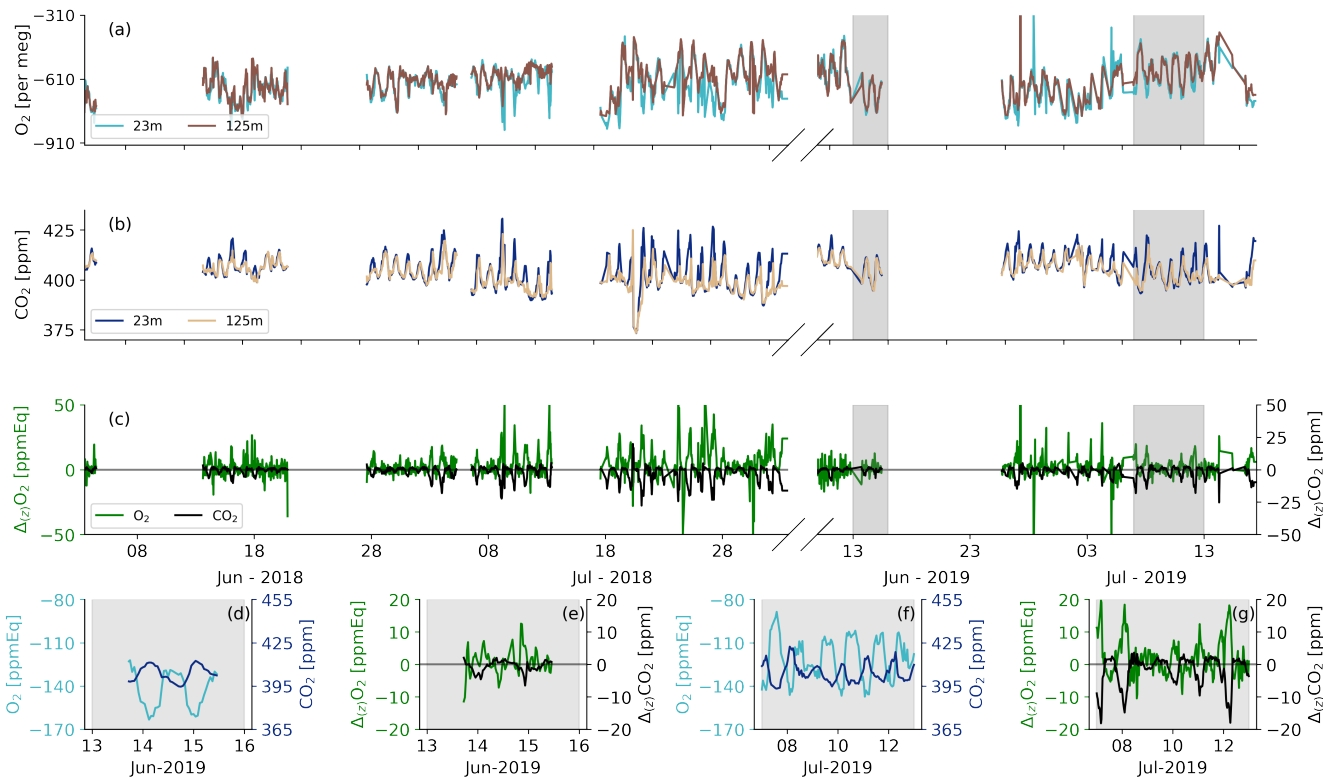
Figure 3. The half hourly average O_2 (a) and CO_2 (b) concentrations at Hyytiälä for spring/summer of 2018 and 2019 for the 125 m and 23 m height levels, together with the vertical gradient ($\Delta_{(z)}$) between these two heights (c) for both O_2 and CO_2. The shaded areas indicates the dates that were selected for the aggregate representative day (7 through 12 July 2019) and the second representative day to test the O_2 method (13 through 15 June 2019). The selected days for the aggregate representative days are shown in more detail for the 23 m measurements and the gradients for 13 through 15 June (d) and (e) and for 7 through 12 July (f) and (g) for both O_2 and CO_2.

July we used a fixed calibration time, as radiosondes were launched (not shown) during this period and we wanted to make sure we captured the morning transition to compare with these radiosondes. Note that the daylight length at Hyytiälä is long at this time of the year, with sunrise at 03:00 and sunset at 22:00. We compared our CO_2 observations with ICOS CO_2 measurements at the same height, which shows that both instruments compare well overall, with a mean difference of 0.70 ± 0.65 ppm during

365   the period 7 through 12 July. The comparison between the two devices was a bit difficult because of the different timing of the measurements. The diurnal cycles of O_2 and CO_2 (Figure 4a) clearly show anti-correlated behaviour between CO_2 and O_2, which is especially visible during nighttime (23:00 - 04:00) and the morning transition (05:00 - 13:00).

Figure 4 shows four different periods that can be linked to the periods to calculate ER_{atmos}, described in section 2.3. P1

370   is visible between 23:00-04:00, where respiration starts to dominate the signal and therefore the O_2 concentration decreases and the CO_2 concentration increases, in a decreasing boundary layer height dominated by thermal stratification. P2 becomes
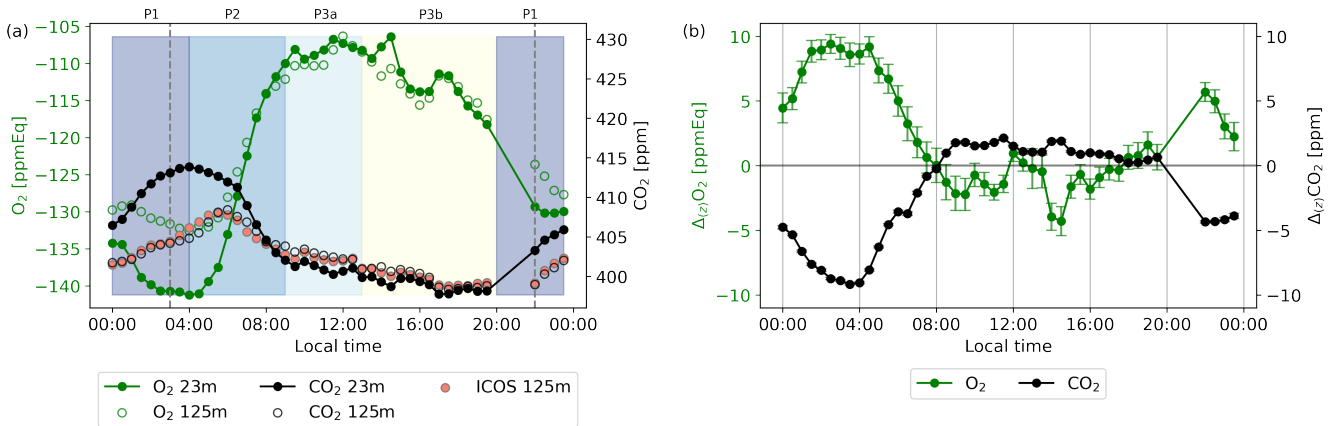
Figure 4. Diurnal cycles (in local wintertime, +2UTC) of the O_2 and CO_2 concentrations for the 23 m and 125 m height levels (a) and the vertical gradient between both levels with the uncertainty of both O_2 and CO_2 of the representative day, taken as the average values of 7 through 12 July 2019 (b). The CO_2 measurements of the ICOS setup are shown in (a) for comparison to the CO_2 setup measured during our campaigns. The shaded colors indicate the selected different periods where the most dominant processes are: stable atmosphere and respiration (00:00-04:00, P1), entrainment, boundary layer growth and assimilation (04:00-09:00, P2), convective conditions and assimilation (09:00-13:00, P3a), the same as P3a, plus a remaining artefact for the O_2 measurements after the pressure correction as explained in the text (13:00-20:00, P3b). The vertical dotted lines indicate the sunrise (3:00) and sunset (22:00). The error bars in panel (b) are half-hourly standard errors based on the error propagation of the standard errors of the data points in (a) (not shown), which were based on equation 4.

visible around 04:00 and stops around 09:00, where entrainment, the growing boundary layer and the onset of photosynthesis causes a steep increase in the O_2 concentration and a steep decrease in the CO_2 concentration. P3 can be divided into P3a and P3b and is visible between 09:00-20:00. Between 09:00-13:00 (P3a), the photosynthesis flux starts to dominate and both
375 the O_2 and CO_2 concentration increase and decrease less rapidly. Between 13:00-20:00 (P3b) the O_2 concentration starts to decrease, while the assimilation flux still dominates, which is a remaining artefact from the pressure correction that we applied due to the instability of the MKS pressure transducer (see Section 2.2). As shown in Figure B1 in Appendix B, higher daytime temperatures cause larger PMKS deviation and therefore the effect of the pressure correction is largest during the mid-day, leading to a larger uncertainty in the observations in that time period. The boundary of 20:00 between P3b and P1 was difficult
380 to determine because we missed some measurements due to the calibration period and the remaining measurements around this time have a deviation caused by the pressure transducer. Measurements at both levels show this same diurnal behaviour, however it is more pronounced closer to the vegetation (the 23 m level).

The difference between the two heights results in a vertical gradient (Figure 4b). Similar to the diurnal cycle of the concen-
385 trations, the diurnal cycles of the gradients of O_2 and CO_2 also show anti-correlated behaviour. At 08:00, the CO_2 gradient changes from negative to positive and the O_2 gradient changes from positive to mostly negative, reflecting CO_2 being transported downwards and O_2 upwards respectively. The magnitude of the gradient depends on the degree of vertical mixing. The

sign of the gradients changes during the day, because the lowest level (23 m) is more directly influenced by forest carbon exchange compared to the highest level (125 m). Around the time of sunset, the CO_2 gradient changes from positive to negative and the O_2 gradient changes from negative to positive, because the lowest measurement level (23 m) is now influenced more by respiration processes of the forest and soils compared to the highest measurement level (125 m). The error bars are based on the error propagation of the standard errors of each half-hourly data point, that were calculated with equation 4. The gradient of O_2 is hardly affected by the PMKS correction (see Figure B1), as measurements at both the heights are affected similarly.
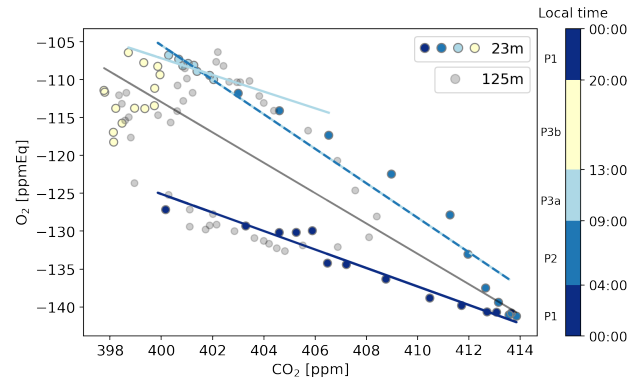
Figure 5. The O_2 concentration plotted against the CO_2 concentration for the representative day (in local wintertime, +2UTC), with the 23 m level in coloured points per period representing different dominant process and the 125 m level in grey points. The dominant processes are: respiration (00:00-04:00), entrainment (04:00-09:00), assimilation (09:00-13:00), a remaining artefact after the pressure correction due to the instability of the MKS pressure transducer becomes visible (13:00-20:00). The linear regression lines indicate the exchange ratio of the atmosphere (ER_{atmos}) during the time with a specific dominant process.

By using equation 5, we calculated four distinct ER_{atmos} signals for different periods throughout the day at 23 m, and to a smaller degree at 125 m (Figure 5 and Table 3). The same periods as shown in Figure 4 are visible in Figure 5. This results in an ER_{atmos} during the night (P1) of 1.22 ± 0.02 and two different possibilities for the ER_{atmos} signal during daytime. By combining both P2 and P3a we get a signal of 2.28 ± 0.01 and by focusing only on P3a, which excludes the entrainment and the boundary layer dynamics, we get a signal of 1.10 ± 0.12. Last, by combining all the periods (P1, P2, P3) we get a signal for the complete day of 2.05 ± 0.03. The uncertainties given here only represent the uncertainty of the slopes from the regression lines in Figure 5. The high values for the ER_{atmos} signal of the entire day and the daytime signal that includes entrainment and the boundary layer dynamics are not very realistic to represent an ER for the forest, and shows that we should be careful when using ER_{atmos}. This will be elaborated on in Section 4.2.
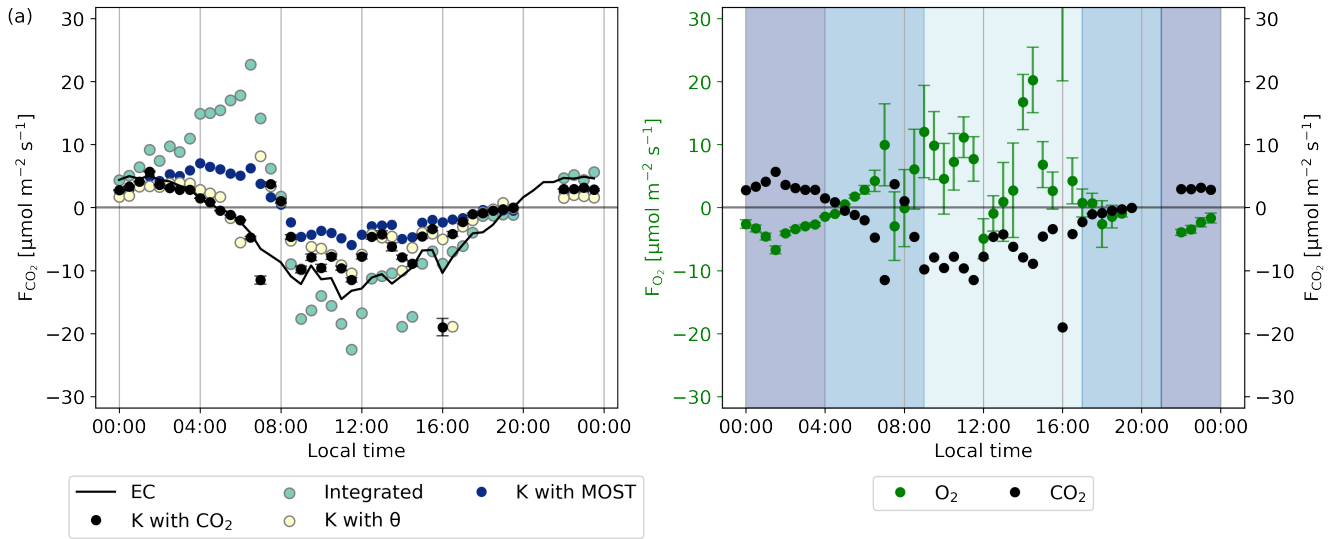
Figure 6. The CO_2 flux (a) calculated with different methods for the representative day, as described in Section 2.3, compared to the CO_2 flux of the ICOS EC measurements. (b) The comparison between the O_2 and CO_2 flux calculated using the method that gave the best results for the CO_2 flux calculations (using the exchange coefficient K with CO_2), for the representative day. The shaded colours indicate the regions that were selected for: the night signal (21:00-04:00), the day signal (09:00-17:00) and the remaining regions (04:00-09:00 and 17:00-21:00), with the time in local wintertime, +2UTC. The error bars of (b) are based on the error propagation of the standard error of the 30-minute values for the representative day, which are based on Equation 4.

3.3 Flux calculations for CO_2 and O_2

We explored four alternative methods to derive the O_2 flux from the vertical gradient of the two measurement levels, as described in Section 2.3. Figure 6 shows both the theoretical and the observation-based approach that were used to calculate the CO_2 flux and the comparison with the ICOS EC CO_2 flux measurements at 27 m on the tower. By comparing these approaches to the EC measurements, we determined which method is most suitable to calculate the O_2 flux. The CO_2 flux measured by the EC system stays positive until around 05:00, when the respiration fluxes are the most dominant and the nocturnal boundary layer is shallower. After 05:00, the CO_2 flux of the EC system becomes negative, and the forest begins to take up CO_2 instead of emitting it. The assimilation fluxes increase and exceed the respiration fluxes, the boundary layer starts to grow and air with lower CO_2 concentrations is entrained from the free troposphere. After 20:00, the CO_2 flux of the EC system becomes positive again because the assimilation fluxes decrease, and the respiration signal begins to dominate again while the boundary layer height decreases. We expect to find this diurnal pattern and the sign change in our calculations of the CO_2 flux from the vertical gradient method as well.

First, we discuss the theoretical methods that are indicated in Figure 6 with 'K with MOST' and 'Integrated' approach (see Section 2.3). The MOST and the Integrated method both overestimate the CO_2 flux during the night, between 0:00 and 05:00.

420 In addition the resulting CO_2 flux decreases and becomes negative too late in the day compared to the EC measurements. Both the CO_2 flux of the MOST and Integrated method evolve from a positive flux to a negative flux around 8:00. This is three hours later than the CO_2 flux from the EC measurements. During the day, between 08:00 and 15:00, the MOST method underestimates the CO_2 uptake and the Integrated method overestimates it. Table 2 shows that both MOST and the Integrated method have the highest mean difference and Root Mean Square Error (RMSE) compared to the observation-based approaches. We dis-

425 cuss this further in section 4.3. As result of this analysis, we decided to not use the theoretical approach to calculate the O_2 flux.

Table 2. The mean difference and the Root Mean Square Error (RMSE) of the comparison between the EC CO_2 flux measurements at 27 m in the tower and the CO_2 flux calculated with different methods for the exchange coefficient K, based on the ICOS data, each using the vertical gradient of CO_2 at 23 m and 125 m of our campaign data.

Approach for K	Mean difference $[\mu\text{mol m}^{-2}\text{ s}^{-1}]$	RMSE $[\mu\text{mol m}^{-2}\text{ s}^{-1}]$
Integrated	5.21	7.81
K with MOST	4.98	5.83
K with θ	3.71	4.83
K with CO_2	2.80	3.88

Secondly, we analyze the observation-based approaches, that are indicated in Figure 6 with 'K with θ' (where K is established using ICOS vertical gradients of potential temperature and the sensible heat flux) and 'K with CO_2' (where K is established using ICOS CO_2 vertical gradients and CO_2 EC data). The observation-based approaches showed a better comparison with the

430 EC observations in determining the CO_2 flux compared the to theoretical approach. Both the θ and the CO_2 method represent satisfactorily the nocturnal CO_2 flux between 0:00 and 5:00. After 5:00, the fluxes calculated by both methods start to decrease and change sign around the correct time (5:00) from a positive to a negative flux. During the day between 8:00 and 15:00, both the θ and the CO_2 methods underestimate the CO_2 flux, but not as much as the theoretical methods. Table 2 also shows that both the θ and the CO_2 methods have the lowest Mean difference and RMSE. Based on the smaller mean difference and

435 RMSE, and the direct link of CO_2 with O_2, we decided to proceed with the method where K is calculated with the ICOS data of CO_2, instead of the ICOS θ data. This K was then multiplied with our measured O_2 vertical gradient between 23 m and 125 m to calculate the O_2 flux. Section 4.3 presents a more complete discussion on the different methods to determine the most suitable K.

440 The resulting O_2 flux calculated with the exchange coefficient K based on the ICOS CO_2 data is shown in Figure 6b. The uncertainties are based on the error propagation of the standard errors of the O_2 and CO_2 data per time step as calculated with

equation 4, in equation 7. We do not calculate an uncertainty for K, as this is not the dominating term contributing to the total uncertainty. The daytime flux values have a high variability, but the inferred fluxes appear physically realistic and promising for one of the first attempts to calculate O_2 fluxes. During the night, between 0:00 and 5:00, the O_2 flux data has a relatively stable negative value, because the forest consumes O_2 for the respiration processes. Similarly CO_2 is released during the night, leading to a positive CO_2 flux. After 5:00, the O_2 flux becomes positive and shows a higher variability. Overall, the O_2 flux is positive during the day which indicates that the forest produces O_2 because the assimilation rate is higher then the respiration rate. The high variability of the O_2 flux compared to the CO_2 flux is caused by the less precise measurements of the O_2 vertical gradient compared to the CO_2 gradient (Figure 4). The measurement precision needed to measure the difference between the two levels is very high, and therefore impacts the measurement of the gradient of O_2. The nighttime values of the O_2 flux are therefore more reliable than the daytime values, since the difference between the two heights is larger and due to the more stable atmospheric conditions at night.
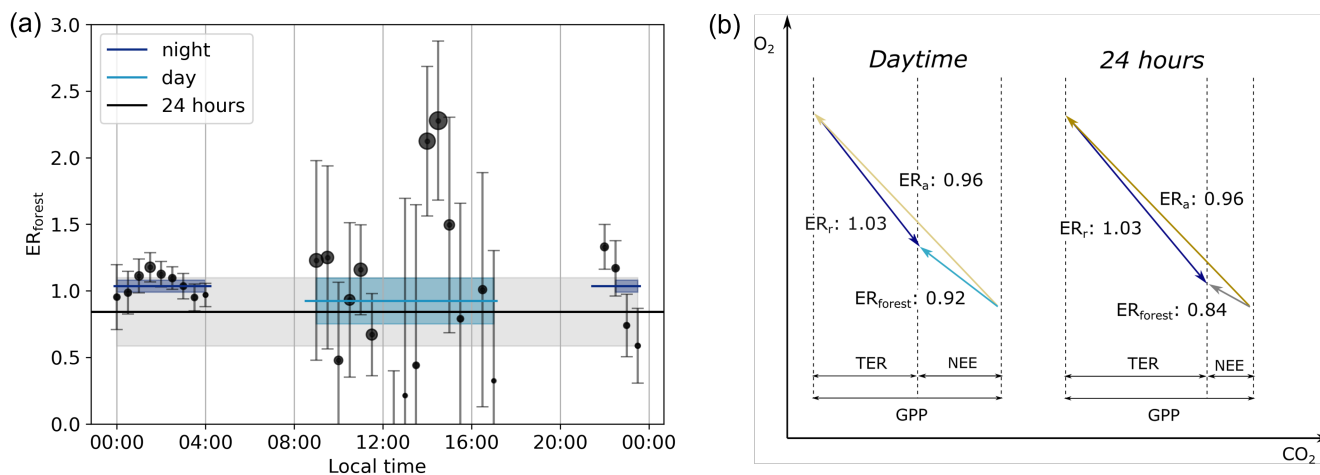
Figure 7. The half-hourly exchange ratio of the forest (ER_{forest}) and the resulting averaged ER_{forest} for the entire day (black line), the night between 21:00-4:00 (dark blue line) and the day between 9:00-17:00 (light blue line), of the representative day (a) with the time in local wintertime, +2UTC. The size of the dots indicates the size of the absolute O_2 flux and the shaded bands indicate the uncertainties of the different ER_{forest} signals. Note that the ER_{forest} lines do not match with the average of the dots in the specific time period, because the lines are based on the averaged fluxes. These different ER signals are presented in a vector diagram format with the carbon fluxes, Gross Primary Production (GPP), Total Ecosystem Respiration (TER) and Net Ecosystem Exchange (NEE), and the ER of the assimilation processes (ER_a) and the ER of the respiration processes (ER_a) (b).

By using equation 6, we find three different ER_{forest} signals throughout the day (Figure 7 and Table 3). The selected time periods based on the criteria described in Section 2.3 are between 09:00-17:00 for the daytime and between 21:00-04:00 for the nighttime (Figure 6). This results in a nighttime ER_{forest} signal of 1.04 ± 0.04, a daytime ER_{forest} signal of 0.92 ± 0.17 and

an ER_{forest} signal for the entire 24 hours of 0.83 ± 0.24. Note that this 24h value is not the average of the day and night ER_{forest} signals or from all the 30-minute ER_{forest} signals, because we used the averaged fluxes. This means that the ER_{forest} signals based on high flux values, indicated in Figure 7 with larger symbols, contribute more to the averaged ER_{forest} signals compared to the lower flux values. Figure 7b illustrates that when combining surface fluxes with different sign, we cannot just average the corresponding ER signals (see Section 4.4). The individual ER_{forest} values of every 30-minutes show a clear difference between the day- and nighttime. The ER_{forest} values during the nighttime are relatively stable. The ER_{forest} values during the daytime show more variability, caused by the high variability of the O_2 flux during daytime (Figure 6). The uncertainty of the ER_{forest} signals is determined by the propagation of the standard error of the aggregate 30-minute data (based on equation 4), in equations 7 and 6.

3.4 GPP and TER calculations

Table 3. The exchange ratio for the atmosphere (ER_{atmos}: Section 3.2), the forest (ER_{forest}: Section 3.3), and assimilation and respiration (ER_a and ER_r: section 3.3) for different time periods of the representative day. The time periods used to calculate the signals are: (09:00-13:00) for day and (23:00-04:00) for night of ER_{atmos}, and (09:00-17:00) for day and (21:00-04:00) for night of ER_{forest}, ER_r and ER_a. Note that the uncertainty for ER_{atmos} does not represent the same uncertainty as for ER_{forest}, since the first is the error of the fit, and the second is based on error propagation of the half hourly measurements.

	ER_{forest}	ER_r	ER_a	ER_{atmos}
Night	1.03 ± 0.05	1.03 ± 0.05		1.22 ± 0.02
Day	0.92 ± 0.17	1.03 ± 0.05	0.96 ± 0.12	1.10 ± 0.12
24 hours	0.84 ± 0.26	1.03 ± 0.05	0.96 ± 0.11	2.05 ± 0.03

We found the ER signals for assimilation (ER_a) and respiration (ER_r) by using equation 9 (Figure 7b and Table 3). The assumption that ER_r stays constant throughout the day seems reasonable, because the ER_{forest} values stay stable during the night. A more elaborate discussion of this assumption can be found in Section 4.5. Therefore the ER_r signal becomes 1.03 ± 0.05. ER_a of the daytime is 0.96 ± 0.11, which indicates the ER_a signal of the boreal forest when the surface fluxes are the highest. The ER_a signal of the entire diurnal cycle is 0.95 ± 0.11, which also includes the assimilation processes during sunrise and sunset. Figure 7b shows all these ER signals and how they change throughout the day, together with their carbon fluxes. ER_a, ER_r and the resulting ER_{forest} signals are more realistic compared to the ER_{atmos} signals. We will elaborate on these differences in Sections 4.4 and 4.5.

By using equation 8 and 9 for a second representative day (13 through 15 June), with the ER_a and ER_r signals determined from the representative day, we show in Figure 8 that the O_2 method compares well with the EC method. This means that the O_2 method could potentially be used to separate NEE into GPP and TER on any day where good simultaneous CO_2, O_2 and
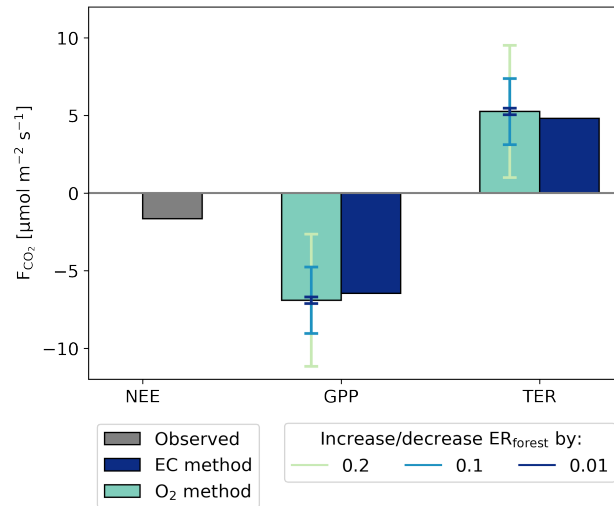
Figure 8. The CO_2 fluxes of a second representative day (13 through 15 June) for Net Ecosystem Exchange (NEE), Gross Primary Production (GPP) and Total Ecosystem Exchange (TER) based on two different methods: the EC method and the O_2 method. The different error bars indicate an increase/decrease of 0.2, 0.1 or 0.01 for the Exchange Ratio of the forest (ER_{forest}), used in the O_2 method.

480 NEE measurements are available. The difference between the CO_2 fluxes determined with the O_2 method and the EC method of both the GPP and the TER flux are around 0.5 μmol m^{-2} s^{-1}, which is less that 6% of the total gross flux. The difference is relatively small which means that the O_2 method compares well with the EC methods to separate NEE into GPP and TER. The different error bars in Figure 8) show how sensitive the O_2 method is to the accuracy of ER_{forest}. By changing ER_{forest} with 0.2, the GPP estimation by the O_2 method changes by 4 μmol m^{-2} s^{-1} and by changing ER_{forest} with only 0.01, the GPP

485 estimation changes with 0.2 μmol m^{-2} s^{-1}. The effect of changing ER_{forest} on TER has the same effect on GPP. This shows that the O_2 method is quite sensitive to ER_{forest} and should be measured accurately, with a suggested precision of around 0.05. With a precision of 0.05 for ER_{forest} the GPP and TER fluxes derived with the O_2 method stay in the same range as the GPP and TER fluxes determined with the EC method. The application of the O_2 method will be further discussed in Section 4.5.

4   Discussion

490 We aimed to advance understanding of the $O_2 : CO_2$ exchange ratio and its diurnal variability over a boreal forest by continuously measuring both O_2 and CO_2 concentrations at two heights above the canopy. These measurements gave us the possibility to compare the ER_{atmos} and ER_{forest} signal of an aggregate representative day and compare the boreal forest signals to previous studies in different ecosystems. Our ER_{atmos} signal changed between the day (2.28) and the night (1.22) and had an overall diurnal signal of 2.05. For the ER_{forest} signal, we needed to determine the O_2 and CO_2 surface fluxes based on the two heights.

495 Different flux calculating methods were compared. The O_2 flux was calculated with the method that resulted in the best comparison to EC fluxes for CO_2, where we found that the exchange coefficient K based on the CO_2 data was most suited. The

resulting ER_{forest} signal showed again differences between the day (0.92) and night (1.04) and the overall diurnal ER_{forest} was 0.83. For these differences and variability in the ER signals, different aspects of the uncertainty have to be taken into account, on which we elaborate in the next sections.

4.1 Measurement uncertainty

Analyzing the mean difference and standard deviation of the target cylinder values between 16-06-2019 and 17-07-2019 (Table 1), we see that the values are relatively high. Previous studies that used a fuel cell analyser for continuous atmospheric O_2 measurements (Battle et al., 2019; Ishidoya et al., 2013; van der Laan-Luijkx et al., 2010; Popa et al., 2010; Pickers et al., 2022), achieved measurement precision of around 5 per meg. WMO recommends a compatibility goal of 2 per meg, however this is difficult to achieve and therefore the extended compatibility goal is 10 per meg for the world-wide O_2 monitoring network (Crotwell et al., 2020), which shows that our long-term measurement precision of 19 per meg is relatively poor. This poor measurement precision could have been caused by several reasons; the O_2 values of the calibration cylinders that were used were relatively far apart, making it more difficult to measure the values around the target cylinder value. For 2018 we used calibration cylinders with the following values (on the SIO scale): -628.53 per meg -816.17 per meg, and -1208.28 per meg and for 2019 we used cylinders with values: -729.96 per meg, -816.17 per meg, and -1208.28 per meg. The cabin in which the instrument and cylinders were located was not well insulated, which created unstable temperature conditions which might have affected the stability of the cylinders (Keeling et al., 2007). The calibrations of our representative aggregate day took place during the night and therefore large temperature changes during the day might have affected daytime stability of the reference cylinder. Furthermore, tiny leakages in the setup might have influenced the measurements. Due to the relatively short period for these campaigns and remote location, it is not possible to trace back the cause of this large uncertainty. This high uncertainty resulted in a larger uncertainty of the vertical gradient of the two heights of the O_2 measurements. However, in this study we are mostly interested in the diurnal variability of the ER signal and differences between ER_{atmos} and ER_{forest} and therefore the long-term stability of the measurements are less relevant here compared to other O_2 studies.

To reduce the effect of the high measurement uncertainty and derive a more statistically robust signal of the vertical gradient, we created an aggregate representative day based on days with similar weather and atmospheric conditions. The increased statistics of this representative aggregate day decrease the effect of the low measurement precision. We also move away from the reality of one specific day, but rather focus on an average situation and variability of the ER signal above a boreal forest based on O_2 and CO_2 measurements at 2 levels. Given that very few previous studies focused on deriving forest ER signals globally, our analysis helps to gain further understanding of the diurnal variability and the difference between ER_{atmos} and ER_{forest}, which will be discussed in the following sections.

4.2 ER_{atmos} signal in comparison to previous studies

Despite the uncertainty in our measurements, there are clear differences between the slopes of O_2 and CO_2 throughout the diurnal cycle (Figure 5). Three different ER_{atmos} signals are visible, with two signals for the day (2.28 ± 0.01 and 1.10 ± 0.12)

530 and one for the night night (1.22 ± 0.02) slope (Table 3). Note that the uncertainty of these values is based on the slope of the fitted line in Figure 5 and does not represent the uncertainty in the stability of our measurements indicated in Table 1. The difference between day and night values of ER_{atmos} was expected because different processes (i.e. respiration, assimilation and entrainment) with different ER signals play a role at different times during the diurnal cycle. To exclude as much as possible the effect of entrainment and the boundary layer dynamics during the morning transition, we will from now on refer to the 1.10

535 value as the day ER_{atmos} signal, which is the signal derived form period P3a. ER_{atmos} for the complete day results in 2.05 ± 0.03.

Table 4. The different Exchange Ratio (ER) signals of previous studies, with the ER of the atmosphere (ER_{atmos}), the ER of the forest (ER_{forest}), the ER of the respiration processes (ER_r) and the ER of the assimilation processes (ER_a). The different studies are: Bat, 2019: (Battle et al., 2019), Ish, 2015: (Ishidoya et al., 2015), Ish, 2013: (Ishidoya et al., 2013), Sei, 2004: (Seibt et al., 2004).

| Study | ER_{atmos}[a] | | | ER_{forest}[b] | | | ER_r | ER_a |
	Day	Night	24 hours	Day	Night	24 hours		
This study	1.10 ± 0.12	1.22 ± 0.02	2.05 ± 0.03	0.92 ± 0.17	1.03 ± 0.05	0.84 ± 0.26	1.03 ± 0.05	0.96 ± 0.12
Bat, 2019	1.02 ± 0.01	1.12 ± 0.01						
Ish, 2015				< 1.0	> 1.0	0.86 ± 0.04	1.11 ± 0.01	1.0
Ish, 2013	0.87 ± 0.02	1.03 ± 0.02	0.94 ± 0.01	≈ 0.98	≈ 1.11	0.89	1.11 ± 0.01	1.02 ± 0.03
Sei, 2004[c]			1.01 ± 0.06	1.24 ± 0.06	1.01 ± 0.02	1.26 ± 0.05	0.94 ± 0.04	1.19 ± 0.12
Sei, 2004[d]	1.14 ± 0.19	1.16 ± 0.02	1.03 ± 0.05					

[a] An ER signal is classified as ER_{atmos} when the ER signal is based on one concentration measurement of O_2 and CO_2.

[b] An ER signal is classified as ER_{forest} when the ER signal is based on surface fluxes from either an 1-box model or vertical gradient flux calculations.

[c] The ER signals of the location Griffin Forest of Seibt et al. (2004) are used here.

[d] The ER signals of the location Harvard Forest of Seibt et al. (2004) are used here.

When comparing our ER_{atmos} signals to those from Battle et al. (2019), Ishidoya et al. (2013) and Seibt et al. (2004) (Table 4), we note several similarities but also some differences regarding the specific values of the ER_{atmos} signals. Our daytime signal of 1.10 is similar to 1.02, 0.87 and 1.14 from the previous studies respectively, as is our nighttime signal of 1.22 compared to

540 1.12 (Battle et al., 2019), 1.03 (Ishidoya et al., 2013) and 1.16 (Seibt et al., 2004). However, our 24-hours ER_{atmos} signal of 2.05 shows an unrealistically high number which clearly does not indicate the ER of the forest only. A typical ER_{atmos} signal for a 24 hour period lies around 1, as is shown in table 4 and by Stephens et al. (2007) and Manning (2001). Our 24-hours ER_{atmos} value includes the measurement points of the period that is influence by entrainment and boundary layer dynamics (P2), for which period we found an ER signal of 2.28. The large influence of entrainment and boundary layer dynamics made it difficult

545 to be very precise about the specific time periods to choose for P3. Moving the selected time boundaries of P3a from 9:00 to 9:30 or from 13:00 to 12:30 leads to ER_{atmos} values of 0.88 or 1.75 respectively. The large changes in the daytime ER_{atmos} due to small changes in the time boundaries, shows the high uncertainty of the daytime ER_{atmos}. Therefore, our measurements provide a confirmation of earlier indications (Seibt et al., 2004) that ER_{atmos} is an unreliable estimate for the ER of a forest,

and we recommend to use ER_{forest}.

550

Instead, ER_{atmos} also represents how O_2 and CO_2 are influenced by the boundary layer dynamics and entrainment (Figure 1). The high ER_{atmos} values cannot be explained by signals from other sources, such as fossil fuel combustion or exchange with the lake, as both are not represented in the footprint of our measurements (see Section 2.3). Furthermore, we have shown that these high values are not an artefact from the instability of the pressure stabilization, as preliminary analysis of the ER_{atmos}

555 values from our 2018 measurements also show values higher than 2.0 (not shown). Although we cannot fully rule out remaining artefacts in the calibration due to e.g. temperature changes in the measurement cabin, we suggest that the more plausible explanation is that ER_{atmos} is highly influenced by atmospheric processes, such as entrainment. The entrainment of air from either the residual layer (early in the morning transition) or the free troposphere (after the residual layer is dissolved) could impact the ER_{atmos} as different sources of air are mixed. The residual layer contains air from the day before and could be affected

560 by horizontal advection whereas the air in the free troposphere originates from different background sources. These difference sources can have different ER signals and therefore create a mixture of air where O_2 and CO_2 are influenced differently. These air masses affect O_2 differently compared to CO_2 in the boundary layer and an ER_{atmos} signal will arise that cannot be linked directly to one specific process. Even though entrainment processes also occur at locations of previous studies, we still find differences in ER_{atmos}. We suggest that this can be explained by difference in measurement height compared to the canopy

565 height and different sources of background air in the free troposphere at the measurement location. For the ER_{atmos} signal during P2 at 125 m, we find a value of 3.40, even higher than the ER_{atmos} signal of 2.28 at 23 m, which indicates the influence of entrainment increases when measuring further away from the canopy and as a result the ER_{atmos} signals shows higher values. Further insights on the contributions of each process to ER_{atmos} cannot be estimated from the measurements alone, and would require using an atmospheric model.

570

4.3 Uncertainties in the CO_2 and O_2 flux calculations

By comparing the theoretical and observation-based methods, we determined that the most suitable method to calculate both the CO_2 and O_2 flux was to use the observation-based method with CO_2 data (Section 3.3). Figure 6 and Table 2 show that the theoretical methods (MOST and Integrated) resulted in a change of the CO_2 flux that was late compared to the EC-measurement.

575 This delay has been described before and is caused by the time it takes before the turbulence can mix the CO_2 gradient driven by stable nocturnal stratification conditions and establish the corresponding gradient to how turbulent the atmosphere is (Casso-Torralba et al., 2008). When the heights of the gradient are closer together, the delay is less pronounced. However, the measurement heights used during our campaign are relatively far apart (125 m and 23 m) and the EC flux is measured at 27 m. The 125 m measurement is even located outside the surface layer during the morning transition. This made the flux-gradient

580 method (as described in Equation 7) less applicable, which assumes that the surface flux stays constant in the surface layer (Dyer, 1974).

Since during our campaign we only measured at two heights, we missed information on the logarithmic profile originating from the canopy top, which resulted in an underestimation of the flux using the K with MOST. This was solved by integrating the MOST equation ('Integrated method'). With the integrated method, the gradient is assumed to be logarithmic and the total flux increases compared to the MOST calculation (Paulson, 1970). However, with the large difference between the two measurement heights, the integrated approach still overestimated the CO_2 flux compared to the EC measurements during both the day and the night. Also, the delay in the timing of the sign change of the gradient cannot be solved with this Integrated method. We also explored the effect of adding a Roughness Surface Layer (RSL) in the flux calculations of the theoretical methods, by adding an extra factor that accounts for this layer (not shown in the results) (de Ridder, 2010). The contribution of the RSL did not improve our results, because it also includes the delay of the gradient which was causing the largest deviation in the theoretical methods (Table 2).

By applying both observation-based methods, using either θ or CO_2 to infer the exchange coefficient K, we did not find this delay in the timing of the gradient and the observation-based methods therefore resulted in derived fluxes close to the EC measurements. Here it has to be noted that the ICOS EC measurements of CO_2 that we used as a benchmark for the most suitable flux calculation approach, was also used in calculating K with CO_2, which makes the comparison of these approaches to the CO_2 flux not fully independent. Note that we first derive K with the vertical CO_2 gradients calculated from ICOS CO_2 observations at three vertical levels, and apply this to our own measurements of the CO_2 vertical gradient with an independent instrument (Table B1). As a result there is not a full circularity when comparing the obtained fluxes to the EC CO_2 measurements to select which method for calculating K we use. Most previous studies that determined fluxes based on the gradient-approach used θ to calculate K (Stull, 1988; Mayer et al., 2011; Wolf et al., 2008; Bolinius et al., 2016; Brown et al., 2020), because θ is the driver of convective turbulence. However, because O_2 is directly linked to CO_2 and our statistics (Table 2) indicated that the CO_2 method resulted in a better comparison to the EC fluxes, we decide to use the ICOS CO_2 data at 3 levels and the CO_2 EC measurements to calculate K. This K together with the measurements of two heights by our instrument during our campaign were used to calculate both the CO_2 and the O_2 fluxes used in our study. We also tested the impact of using only 2 vertical levels of the ICOS CO_2 concentrations to calculate K (not shown), which was also the case in the only previous study that derived O_2 fluxes. Ishidoya et al. (2015) derived O_2 fluxes for a temperate forest in Japan using 2 vertical levels at 18 and 27 m height for both O_2 and CO_2 concentrations. Our comparison of deriving K based on 2 vertical levels (23 m and 125 m), resulted in an underestimation of the gradient and thus an overestimation of K, and as a consequence the calculated CO_2 flux was overestimated. Therefore the 3 levels of ICOS CO_2 concentrations measurements proved to be vital in our flux calculations here. We still missed the logarithmic profile at the surface with only the two vertical campaign measurements and as a result slightly underestimated the final CO_2 and O_2 flux. Therefore, we recommend to always measure at at least three heights of CO_2 and O_2 inside the surface layer, when they are meant to be used for flux calculations.

Our final O_2 flux (Figure 6) shows a clear diurnal cycle, with the expected behaviour of negative values in the night (O_2 consumption for respiration) and a positive flux during the day (O_2 release during assimilation). The nighttime fluxes are more

stable and give a clear signal due to the larger vertical gradient. K is more difficult to determine during the night because the EC measurements are less representative due to the low level of turbulence. However, the largest contributor to the uncertainty are our own O_2 measurements and the larger gradient allows to better establish the O_2 flux. The larger variability of the daytime O_2 fluxes is caused by the smaller gradient of the O_2 concentration measurements during the day (Figure 3), when the atmosphere is more well-mixed and the difference between the two heights becomes smaller. The relatively large measurement uncertainty made it difficult to measure these small difference between the two heights and increased the noise in the fluxes. The measurement noise resulted in O_2 gradient variations that were not tied to the CO_2 gradient variations and this degraded the correlation between the two fluxes. Despite this larger variability, we still find a clear diurnal behaviour, which allowed us to calculate ER_{forest}. Note that the uncertainties of the surface fluxes of O_2 and CO_2 are only based on the measurements from our campaigns and we did not include the uncertainties that are related to the calculations of K based on the ICOS data. However, the uncertainty in K is relatively small compared to the other terms in the calculation, and the final uncertainty of estimates is dominated by the measurement uncertainty of O_2. Omitting the uncertainty associated with K therefore leads to a minor underestimate of the full uncertainty.

4.4 ER_{forest} signal compared to previous studies

Our resulting ER_{forest} signal changes throughout the diurnal cycle, with specific daytime (0.92 ± 0.17), nighttime (1.03 ± 0.05) and overall (0.84 ± 0.26) values (Figure 7 and Table 3). The individual nighttime values show a smaller uncertainty due to the already explained effect of the larger gradient during the stable atmospheric conditions of the night. In contrast, the individual daytime values show a larger uncertainty due to the smaller gradient during the unstable atmospheric conditions of the day. We therefore used averaged values for the daytime and nighttime signals to derive the ER_{forest} values. While the daytime signal excludes the entrainment and the boundary layer dynamics during the morning transition, these effects are still included in the overall ER_{forest} signal. Note that the overall 24 hour signal is not the average of the daytime and nighttime signal. The nighttime ER_{forest} signal represents a negative O_2 flux and a positive CO_2 flux, whereas the daytime ER_{forest} signal represents a positive O_2 flux and a negative CO_2 flux. This means that the daytime and nighttime surface fluxes influence the atmosphere differently and therefore these ER_{forest} values cannot be averaged to calculate the overall ER_{forest} signal. By first calculating the average overall O_2 and CO_2 fluxes and then divide these, we derive the overall ER_{forest} signal correctly.

When comparing our ER_{forest} signals to previous studies of Seibt et al. (2004), Ishidoya et al. (2013, 2015) (Table 4) we notice that the difference between the daytime and the nighttime values that we found and the specific values of the different ER_{forest}, have some similarities and some differences. Our results, along with these of Ishidoya et al. (2013, 2015) (night: 1.11 and day: 0.98) show the ER_{forest} signal of the nighttime is being higher than the daytime signal, whereas Seibt et al. (2004) (day: 1.24 and night: 1.01) showed the opposite behaviour. Our results are most similar to the signals of both Ishidoya et al. (2013) and Ishidoya et al. (2015), especially if we take our uncertainty range into account. The 24 hours signals are difficult to compare as we used a different method to determine the overall ER_{forest} signal compared to Ishidoya et al. (2015). In this study

we use average fluxes instead of a linear regression through either the O_2 and CO_2 fluxes or vertical gradient and we thereby take into account the size of the fluxes that contributes most to the ER signal, which results in a flux-weighted average ER_{forest}. We note again that we need to distinguish between daytime and nighttime signal, and we cannot just average them. Figure
655 7 illustrates the need to take averages in consistent meteorological and biological periods that are characterized by similar turbulence regimes and similar signs of the O_2 and CO_2 exchange. For example, combining a small negative O_2 flux with a high ER, with a large positive O_2 flux with a lower ER, results in a smaller O_2 flux, compared to when the ERs of both fluxes would have been the same. When we take into account our uncertainty, the complete day signal of 0.84 ± 0.26 comes close to the globally used average ER of the biosphere of 1.1 (Severinghaus, 1995). However, the specific value suggest that the overall
660 ER_{forest} signal of this boreal forest lies somewhat lower than 1.1, closer to 1.0. The difference in ER_{forest} signals between studies can be explained with the different ER_a and ER_r signals, which we discuss in section 4.5.

The ER_{forest} and ER_{atmos} signals are not identical, and they do therefore not represent the same information (Table 3). The ER_{atmos} signals are higher compared to the ER_{forest} signals, especially the 24-hour signals show a large difference. Despite
665 the higher numbers, the day and night signals of ER_{atmos} and ER_{forest} show both the same pattern, where the daytime signal is lower compared to the nighttime signal. When comparing these differences to previous studies we find that not all studies find the same results. The difference between ER_{forest} and ER_{atmos} was not found by Ishidoya et al. (2013). In contrast, Seibt et al. (2004) found a difference between ER_{forest} and ER_{atmos} (Table 4). A reason for this could be the measurement height of ER_{atmos}. When ER_{atmos} is determined closer to the canopy and inside the roughness sublayer, it will be more influenced by the
670 surface processes compared to measurements at higher levels, which are seeing more integrated signals of all processes that influence the concentrations inside the atmospheric boundary layer (i.e. forest exchange and non-local processes like entrainment). To get a clear answer to this question, we should further investigate to what extent ER_{atmos} is influenced by entrainment and boundary layer dynamics and under which conditions they can come close to ER_{forest}. We already show that excluding the morning transition (P2) helps to improve the ER_{atmos} signal. However, as already stated, it is difficult from the measurements
675 alone to determine if the ER_{atmos} signal is influenced only by the surface during this period. An Atmospheric model would therefore be needed to find how ER_{atmos} can be derived from a single measurement height, and allow comparison to previous studies that measured at one height to determine the ER of the forest (Battle et al., 2019; van der Laan et al., 2014; Stephens et al., 2007). We are currently applying a specific mixed-layer atmospheric model to further investigate this.

680 **4.5 The ER_a and ER_r signals**

To further understand the relationship between O_2 and CO_2, we cannot use the ER_{forest} signal alone. To look in more detail into the processes driving the variations, we calculated the exchange ratios of respiration (ER_r) and assimilation (ER_a) (Table 3 and Figure 7). ER_r was taken as the ER_{forest} night-time signal (1.03 ± 0.05), by assuming that only respiration influences the ER_{forest} signal during the night and that the ER_r signal stays constant throughout the entire day. This means that both the heterotrophic
685 and autotrophic respiration are included in ER_r and the same components are respired in the same ratios throughout the day

to keep ER_r a constant value. The studies that looked at the ER_r of an ecosystem (Hilman et al., 2022; Angert et al., 2015; Hicks Pries et al., 2020) only focused on longer time scales than the diurnal cycle. It is therefore not possible to derive diurnal variability of ER_r from these previous studies. We would expect some changes in ER_r as temperatures changes during the day and the respiration of plants involves photorespiration during daytime and dark respiration during nighttime. However, as the study of Hilman et al. (2022) showed, the variability of ER_r mainly depends on the bulk soil respiration and therefore depends on the soil temperature and soil moisture. No large changes in temperatures or soil moisture were detected during the period of the representative aggregate day, and therefore it is unlikely that the ER_r significantly changed in that period. To get a more detailed view on how the ER_r of an ecosystem changes throughout the day, more research is needed on the variability of ER_r including from plant respiration by chamber measurements.

The variability of ER_r between locations highly depends on the soil properties (Angert et al., 2015), which makes it difficult to compare with the few studies available (Seibt et al., 2004; Ishidoya et al., 2013) that measured ER_r with chamber measurements on a brown soil. The soil in our study area is a podzol, which is characterised by a high acidity with little organic matter (Buurman and Jongmans, 2005). The OR of podzols is around 1.08 (Worrall et al., 2013) and the ER of acid soils is expected to be around this OR, because carbon cannot easily dissolve into the groundwater (Angert et al., 2015), and we therefore conclude that our ER_r value of 1.04 is realistic.

We looked at two options to calculate ER_a; ER_a based only on the daytime measurements (between 9:00 and 17:00: 0.96 $\pm$ 0.12) and ER_a based on all the measurement throughout the 24-hour period: 0.96 $\pm$ 0.11). Both numbers are close to 1, which is often assumed as a standard value for ER_a (Ishidoya et al., 2015; Severinghaus, 1995). Next to that, a value of ER_a close to 1 means that ammonium is used as a source for nitrogen, instead of nitrate (Bloom et al., 1989, 2012). Ammonium is indeed a larger source for nitrogen compared to nitrate in Hyytiälä (Korhonen et al., 2013). The OR of needle leaves, and plant material in general, appears to be always close to 1.0 (Jürgensen et al., 2021), which again confirms our ER_a signals. We did not observe differences between the two ER_a signals. The transition periods between the night and the daytime were difficult to measure, because the gradient then becomes close to zero, which means there could be a possibility that next to ER_{forest}, ER_a also has a diurnal cycle. Again, there are only a few studies that looked at the variability of ER_a (Fischer et al., 2015; Bloom et al., 1989, 2012; Bloom, 2015). The available studies show that ER_a depends on light (Fischer et al., 2015) and the source of nitrogen in the soil (Bloom, 2015). These changes in ER_a happen when the changes in the atmosphere and the soil are sudden and persist for a longer time compared to a diurnal cycle. We can therefore say that the ER_a also does not change drastically during the day. To get a more detailed overview of ER_a, more precise measurements are needed with uncertainties lower than 0.1 for the ER signals. However, the similar values of ER_a that we find for the daytime and 24 hour measurements show that ER_a is hardly affected by entrainment during the morning transition and it would suggest that the morning transition is less of an issue for ER_{forest} than for ER_{atmos}.

By applying the O_2 method to a new aggregate day, we showed that the O_2 method gives results similar to the EC method to partition NEE and derive the GPP and TER fluxes (Figure 8), with estimates of the uncertainties of the O_2 method. The EC method also contains uncertainties in its approach because of the reliance on a function of temperature, and should therefore not necessarily be assumed to be the 'truth' (Reichstein et al., 2005). Despite the uncertainty of both the O_2 method and the EC method, both methods give similar results for the CO_2 flux of GPP and TER. In our comparison of the O_2 and EC methods, there is a minor degree of circularity, as we use the EC GPP estimates to estimate ER_a. By applying it to another representative day, we prevent a full circularity (Table B1). In this campaign, we unfortunately could not determine the ER_a and ER_r signals independently from EC, which would be recommended for a full comparison. This would have been possible by using chamber measurements. We expect only minor changes in ER_a from branch/leaf chamber measurements compared to the values we derived, because our ER_a is in the range of expected values compared to previous studies (e.g. Jürgensen et al. (2021); Bloom (2015); Fischer et al. (2015)). The satisfactory comparison between the O_2 and the EC methods for the partitioning of the fluxes shows the potential of the O_2 method. The largest challenge for this method is to determine ER_{forest} with large enough accuracy, as this value is most variable and most difficult to determine based on the small O_2 gradients that we observed. Figure 8 shows that the ER_{forest} signal should be measured with an uncertainty of 0.05 or less to get results within the uncertainty range of the EC method. When such high accuracy is reached, the O_2 method has the potential to provide an alternative method for the separation of GPP and TER without relying on the regularly used temperature-based function as used for the EC method. Ishidoya et al. (2015) showed similar results, where the O_2 method also produced GPP and TER comparable to the EC method and the magnitude of the GPP and TER fluxes highly depended on the derived ER_a and ER_r signals.

To allow an independent comparison between the flux partitioning with the EC method and the O_2 method, such as was done with using $\delta^{13}CO_2$ by Wehr et al. (2016), we recommend measuring the ER_r and ER_a signals directly with chamber measurements (Seibt et al., 2004; Ishidoya et al., 2013). We also recommend to add at least one additional measurement height for the O_2 and CO_2 concentrations below the canopy to apply the storage correction for both the O_2 and the CO_2 fluxes (Aubinet et al., 2012) and to add a measurement in the free troposphere to better evaluate the effect of entrainment. Despite the high dependency on the accuracy of the ER, this study showed again, as did (Ishidoya et al., 2015), that the O_2 method can be used to get a better understanding of the carbon cycle. To further develop this method we need to expand the O_2 measurements for longer time series and more locations, and analyze how ER_{forest} varies over longer time scales, which can improve the global average value of ER (α_B) of 1.1 as used in global carbon budget studies such as Manning and Keeling (2006).

5 Conclusions

By continuously measuring atmospheric O_2 and CO_2 concentrations at two heights in Hyytiälä, Finland, we gained new insights into the diurnal variability of O_2 and CO_2 above a boreal forest, quantified by interpreting their Exchange Ratio (ER). We showed that the signal based on one measurement height of the O_2 and CO_2 concentrations (ER_{atmos}) is not representative

for the exchange between the forest and the atmosphere only, but instead includes other processes such as entrainment as well. To derive the ER of the forest specifically (ER_{forest}), we first determined the surface fluxes above the canopy of O_2 and CO_2 using the vertical gradient between the two measurement heights. We found that the most suitable method to calculate both the O_2 and CO_2 surface fluxes was to use the exchange coefficient calculated from the Eddy Covariance (EC) CO_2 flux and the vertical gradient of CO_2 measurements at three heights above the canopy. The ER_{forest} signals that resulted from the ratio of the mean O_2 and CO_2 fluxes varied between the daytime (0.92 ± 0.17 mol/mol) and nighttime (1.03 ± 0.05 mol/mol). The different ER_{forest} signals were composed of the ER of respiration (ER_r: 1.03 ± 0.05 mol/mol) and the ER of assimilation (ER_a: 0.96 ± 0.12 mol/mol). With these findings we show improved methods to derive O_2 forest fluxes and to derive the variability in the different ER signals over a representative diurnal cycle. The ER_{forest} signal shows a clear diurnal cycle for this boreal forest and the overall ratio is lower than 1.1 that is used in global carbon budget calculations. Finally, we show that these ER signals can be used to separate Net Ecosystem Exchange (NEE) into Gross Primary Production (GPP) and Total Ecosystem Respiration (TER).

With only a few data sets of continuous measurements of both O_2 and CO_2 concentrations over forests, our data set is of high importance, specifically the availability of measurements at two heights that allow calculation of O_2 and CO_2 fluxes. Our analyses can serve as a starting point for follow up research using coupled land surface-atmosphere models to distinguish and quantify contributions of different processes to ER_{atmos} and ER_{forest} signals. Further understanding of these differences will help to fully exploit the advantages of atmospheric O_2 when unraveling the different components in the carbon cycle.

Data availability. The data used in this study are available from https://doi.org/10.18160/SJ3J-PD38.

Appendix A: Equations to calculate the Exchange Coefficient, K

A1 Observation-based method

The gradient between three points is calculated with the following equation:

$$\overline{\phi}(z) = a \cdot z^2 + b \cdot z + c \tag{A1}$$

$$\left(\frac{\partial \overline{\phi}(z)}{\partial z} \right) = 2 \cdot a \cdot z + b \tag{A2}$$

Where z [m] is the height above the displacement height (d [m]) (d is taken as: $2/3 \cdot$ canopy height), $\overline{\phi}$ is the average variable where the line is fitted through and a, b and c are the resulted fitted parameters. When only two vertical measurements are available, the gradient was determined using finite differences.

 A2   Theoretical approach

For the MOST method, the following equations were used (Physick and Garratt, 1995):

$$K = \frac{\kappa \cdot z \cdot u_*}{\Phi_H(\frac{z}{L})\phi_{rsl}(\frac{z}{L})} \tag{A3}$$

Where K is the exchange coefficient [m^2 s^{-1}], $\kappa = 0.4$ is the von Kármán constant, u_* [m s^{-1}] is the friction velocity, Φ_H [-] indicates the stability function and ϕ_{rsl} [-] indicates the contribution of the roughness sublayer (RSL). The Φ_H was calculated with (Dyer, 1974):

$$\Phi_H\left(\frac{z}{L}\right) = \left(1 - 16\frac{z}{L}\right)^{-1/2} \qquad \text{when z/L} < 0 \tag{A4}$$

$$\Phi_H\left(\frac{z}{L}\right) = 1 + 5\frac{z}{L} \qquad \text{when z/L} > 0 \tag{A5}$$

Where L [m] is the Obukov Length, which was based on the following equation (Dyer, 1974):

$$L = \frac{-u_*^3}{\kappa(\frac{g}{\theta_v})(\overline{w'\theta_v'})} \tag{A6}$$

Where θ_v [K] is the virtual potential temperature, $\overline{w'\theta_v'}$ [K m s^{-1}] is the virtual surface heat flux and g [m s^{-2}] is the acceleration due to gravity. Because the flux was measured close to the canopy, the roughness surface layer (RSL) could become important. The RSL needs an additional length scale (ϕ) and can be calculated with the following equation (de Ridder, 2010):

$$\phi_{HRSL}\left(\frac{z}{z_*}\right) = 1 - e^{-\mu\frac{z}{z_*}} \tag{A7}$$

Here z_* [m] indicates the height of the RSL above the displacement height and we take that as ($2 \cdot$ canopy height-d) and μ is a constant of 0.95 [-].

By integrating equation 7 with equation A3 for K, we get the following equation that was used for the Integrated method (Physick and Garratt, 1995):

$$\phi(z_2) - \phi(z_1) = \frac{(\overline{w'\phi'})}{\kappa \cdot u_*}\left[ln\left(\frac{z_2}{z_1}\right) - \Psi_H\left(\frac{z_2}{L}\right) + \Psi_H\left(\frac{z_1}{L}\right) + \psi_{RSL}\left(\frac{z}{L}, \frac{z}{z_*}\right)\right] \tag{A8}$$

Where Ψ_H [-] are the integrated stability functions for heat and ψ [-] is the integrated function to account for the roughness sublayer (RSL) effect. Ψ_H was calculated with (Paulson, 1970):

$$\left.\begin{array}{l}\Psi_H\left(\frac{z}{L}\right) = 2ln\left(\frac{1+x^2}{2}\right) \\ \qquad x = (1 - 16z/L)^{1/4}\end{array}\right\} \qquad \text{when z/L} < 0 \tag{A9}$$

$$\Psi_H\left(\frac{z}{L}\right) = -5\frac{z}{L} \qquad \text{when z/L} > 0 \tag{A10}$$

805 The function of the integrated RSL length scale (ψ_{RSL}) [-] was calculated with (de Ridder, 2010):

$$\psi_{RSL}\left(\frac{z}{L}, \frac{z}{z_*}\right) \approx \Phi_H\left[\left(1 + \frac{\nu}{\mu z/z_*}\right)\frac{z}{L}\right]\frac{1}{\lambda}ln\left(1 + \frac{\lambda}{\mu z/z_*}\right)e^{-\mu z/z_*} \tag{A11}$$

Where ν and λ are both parameters, taken as 0.5 and 1.5 respectively.

Appendix B: Figures and tables
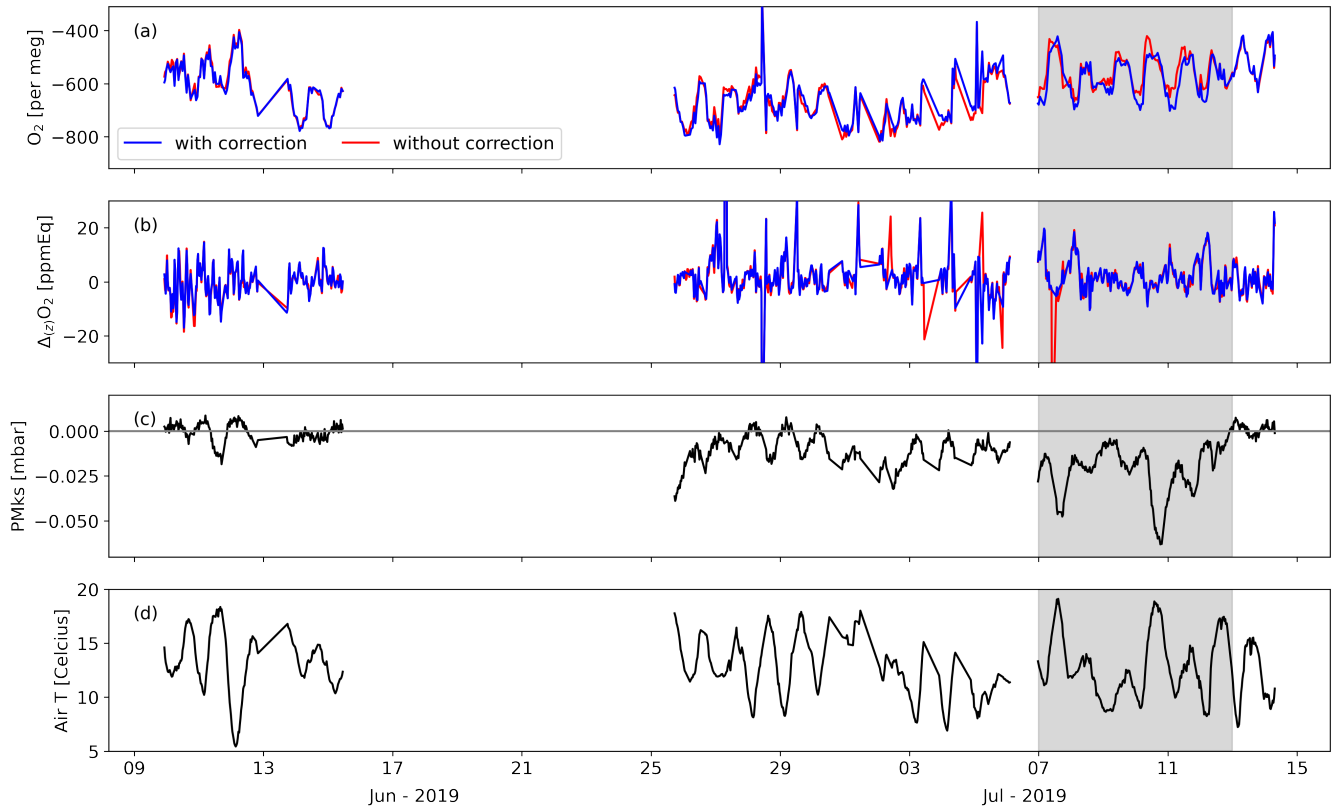
Figure B1. The corrected and uncorrected half-hourly average O_2 concentrations at 23 m for the PMKS deviations (a), together with the corrected and uncorrected gradient of O_2(b). The time series for the 2019 measurement period of the PMKS (c) and the air temperature (d) are also shown. The shaded areas indicates the dates that were selected for the aggregate day, 7 through 12 July 2019.

Table B1. The data used to calculate different variables that we calculated in our study for the two aggregate days. (a) indicates the data that was used for the first representative aggregate day between 7 through 13 July 2019 and (b) indicates the data that was used for the second aggregate day between 13 through 15 June 2019. The data used are mostly from the period of the respective aggregate day, except when indicated otherwise.

(a)	Data used during the analysis of the aggregate day between 7 through 12 July 2019 [a]					
	(1) ER_{atmos}	(2) Exchange coefficient (K)	(3) Surface flux of O_2 and CO_2	(4) ER_{forest}	(5) ER_a and ER_r	(6) GPP and TER
Data used:	· O_2 from campaign at 23 m · CO_2 from campaign at 23 m	· EC CO_2 flux · CO_2 gradient based on three heights from ICOS (125 m, 67 m, 16 m)	· K (2) · CO_2 or O_2 gradient based on two heights from campaign (125 m, 23 m)	· CO_2 flux (3) · O_2 flux (3)	· ER_{forest} (4) · EC CO_2 flux · GPP from ICOS database	-

(b)	Data used during the analysis of the aggregate day between 13 through 15 June 2019 [a]					
	(7) ER_{atmos}	(8) Exchange coefficient (K)	(9) Surface flux of O_2 and CO_2	(10) ER_{forest}	(11) ER_a and ER_r	(12) GPP and TER
Data used:	-	· EC CO_2 flux · CO_2 gradient based on three heights from ICOS (125 m, 67 m, 16 m)	· K (8) · CO_2 or O_2 gradient based on two heights from campaign (125 m, 23 m)	· CO_2 flux (9) · O_2 flux (9)	· ER_a (7-12 July) (5) · ER_r (7-12 July) (5)	· ER_{forest} (10) · EC CO_2 flux · ER_a (5) · ER_r (5)
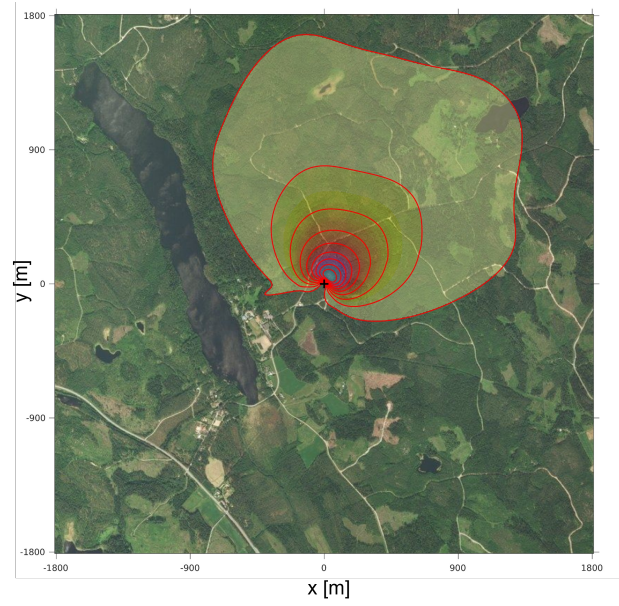
Figure B2. The footprint of the O_2 and CO_2 surface fluxes at 53.6 meters height (which is the geometric height), determined with the gradient method, for the days between 7 through 12 July 2019 at Hyytiälä. The lines and contours indicate the contributions to the footprint from 10% to 90% in steps of 10%. The plus sign (+) indicates the location of the tower.

Author contributions. ITL designed the measurement campaign and conducted the measurements. ITL, ERB, LNTN, PAP and ACM contributed to the design and development of the O_2 and CO_2 measurement setup. LNTN, BAMK, IM and TV contributed to the measurement campaigns. KAPF and ITL analyzed the measurements. KAPF, ITL, WP, JV, HAJM interpreted and discussed the methods and results. KAPF and ITL wrote the manuscript with input from all co-authors.

Competing interests. There are no competing interests.

Acknowledgements. The authors would like to thank Janne Levula (previously worked at Institute for Atmospheric and Earth System Research (INAR) / Physics, Faculty of Science, University of Helsinki, Helsinki, Finland) and Bert Heusinkveld (Meteorology and Air Quality, Wageningen University and Research, Wageningen, the Netherlands) for their help at Hyytiälä during the measurement campaigns, Marcel de Vries (Centre for Isotope Research (CIO), Energy and Sustainability Research Institute Groningen, University of Groningen, Groningen, the Netherlands) for technical support and Charlotte van Leeuwen (previously at Centre for Isotope Research (CIO), Energy and Sustainability Research Institute Groningen, University of Groningen, Groningen, the Netherlands) for the development of the instrument. This work was supported with funding that ITL received from the Netherlands Organisation for Scientific Research (016.Veni.171.095). We thank Üllar Rannik and Pasi Kolari (Institute for Atmospheric and Earth System Research (INAR) / Physics, Faculty of Science, University of Helsinki, Helsinki, Finland) for their work on the interpretation and analysis of the Hyytiälä flux measurements and their footprint. We thank three anonymous reviewers for their comments which helped to improve this manuscript.

References

825 Angert, A., Yakir, D., Rodeghiero, M., Preisler, Y., Davidson, E. A., and Weiner, T.: Using O_2 to study the relationships between soil CO_2 efflux and soil respiration, Biogeosciences, 12, 2089–2099, https://doi.org/10.5194/bg-12-2089-2015, 2015.

Aubinet, M., Vesala, T., and Papale, D.: Eddy covariance: a practical guide to measurement and data analysis, Springer Science & Business Media, 2012.

Ballantyne, A. á., Alden, C. á., Miller, J. á., Tans, P. á., and White, J.: Increase in observed net carbon dioxide uptake by land and oceans

830 during the past 50 years, Nature, 488, 70–72, 2012.

Battle, M. O., William Munger, J., Conley, M., Sofen, E., Perry, R., Hart, R., Davis, Z., Scheckman, J., Woogerd, J., Graeter, K., Seekins, S., David, S., and Carpenter, J.: Atmospheric measurements of the terrestrial $O_2 : CO_2$ exchange ratio of a midlatitude forest, Atmospheric Chemistry and Physics, 19, 8687–8701, https://doi.org/10.5194/acp-19-8687-2019, 2019.

Blaine, T. W., Keeling, R. F., and Paplawsky, W. J.: An improved inlet for precisely measuring the atmospheric Ar/N_2 ratio, Atmospheric

835 Chemistry and Physics, 6, 1181–1184, https://doi.org/10.5194/acp-6-1181-2006, 2006.

Bloom, A. J.: Photorespiration and nitrate assimilation: a major intersection between plant carbon and nitrogen, Photosynthesis research, 123, 117–128, 2015.

Bloom, A. J., Caldwell, R. M., Finazzo, J., Warner, R. L., and Weissbart, J.: Oxygen and Carbon Dioxide Fluxes from Barley Shoots Depend on Nitrate Assimilation, Plant Physiology, 91, 352–356, https://doi.org/10.1104/pp.91.1.352, 1989.

840 Bloom, A. J., Rubio Asensio, J. S., Randall, L., Rachmilevitch, S., Cousins, A. B., and Carlisle, E. A.: CO_2 enrichment inhibits shoot nitrate assimilation in C3 but not C4 plants and slows growth under nitrate in C3 plants, Ecology, 93, 355–367, https://doi.org/10.1890/11-0485.1, 2012.

Bolinius, D. J., Jahnke, A., and MacLeod, M.: Comparison of eddy covariance and modified Bowen ratio methods for measuring gas fluxes and implications for measuring fluxes of persistent organic pollutants, Atmospheric Chemistry and Physics, 16, 5315–5322,

845 https://doi.org/10.5194/acp-16-5315-2016, 2016.

Brown, J., Shapkalijevski, M., Krol, M., Karl, T., Ouwersloot, H., Moene, A., Patton, E., and Vilà-Guerau de Arellano, J.: Ozone exchange within and above an irrigated Californian orchard, Tellus B: Chemical and Physical Meteorology, 72, 1–17, 2020.

Buurman, P. and Jongmans, A.: Podzolisation and soil organic matter dynamics, Geoderma, 125, 71–83, 2005.

Carbon Portal ICOS RI: STILT station characterization for Hyytiälä at 17m, https://hdl.handle.net/11676/sbjAXeKbI09FqHDtFNqf6oVc,

850 2022.

Casso-Torralba, P., de Arellano, J. V. G., Bosveld, F., Soler, M. R., Vermeulen, A., Werner, C., and Moors, E.: Diurnal and vertical variability of the sensible heat and carbon dioxide budgets in the atmospheric surface layer, Journal of Geophysical Research Atmospheres, 113, https://doi.org/10.1029/2007JD009583, 2008.

Cox, P. M., Pearson, D., Booth, B. B., Friedlingstein, P., Huntingford, C., Jones, C. D., and Luke, C. M.: Sensitivity of tropical carbon to

855 climate change constrained by carbon dioxide variability, Nature, 494, 341–344, 2013.

Crotwell, A., Lee, H., and Steinbacher, M.: 20th WMO/IAEA Meeting on Carbon Dioxide, Other Greenhouse Gases and Related Measurement Techniques (GGMT-2019), Tech. Rep. 255, 2020.

de Ridder, K.: Bulk transfer relations for the roughness sublayer, Boundary-Layer Meteorology, 134, 257–267, https://doi.org/10.1007/s10546-009-9450-y, 2010.

860 Dyer, A.: A review of flux-profile relationships, Boundary-Layer Meteorology, 7, 363–372, 1974.

Fischer, S., Hanf, S., Frosch, T., Gleixner, G., Popp, J., Trumbore, S., and Hartmann, H.: Pinus sylvestris switches respiration substrates under shading but not during drought, New Phytologist, 207, 542–550, 2015.

Friedlingstein, P., Jones, M. W., O'Sullivan, M., Andrew, R. M., Bakker, D. C. E., Hauck, J., Le Quéré, C., Peters, G. P., Peters, W., Pongratz, J., Sitch, S., Canadell, J. G., Ciais, P., Jackson, R. B., Alin, S. R., Anthoni, P., Bates, N. R., Becker, M., Bellouin, N., Bopp, L., Chau, T. T. T., Chevallier, F., Chini, L. P., Cronin, M., Currie, K. I., Decharme, B., Djeutchouang, L. M., Dou, X., Evans, W., Feely, R. A., Feng, L., Gasser, T., Gilfillan, D., Gkritzalis, T., Grassi, G., Gregor, L., Gruber, N., Gürses, O., Harris, I., Houghton, R. A., Hurtt, G. C., Iida, Y., Ilyina, T., Luijkx, I. T., Jain, A., Jones, S. D., Kato, E., Kennedy, D., Klein Goldewijk, K., Knauer, J., Korsbakken, J. I., Körtzinger, A., Landschützer, P., Lauvset, S. K., Lefèvre, N., Lienert, S., Liu, J., Marland, G., McGuire, P. C., Melton, J. R., Munro, D. R., Nabel, J. E. M. S., Nakaoka, S.-I., Niwa, Y., Ono, T., Pierrot, D., Poulter, B., Rehder, G., Resplandy, L., Robertson, E., Rödenbeck, C., Rosan, T. M., Schwinger, J., Schwingshackl, C., Séférian, R., Sutton, A. J., Sweeney, C., Tanhua, T., Tans, P. P., Tian, H., Tilbrook, B., Tubiello, F., van der Werf, G. R., Vuichard, N., Wada, C., Wanninkhof, R., Watson, A. J., Willis, D., Wiltshire, A. J., Yuan, W., Yue, C., Yue, X., Zaehle, S., and Zeng, J.: Global Carbon Budget 2021, Earth System Science Data, 14, 1917–2005, https://doi.org/10.5194/essd-14-1917-2022, 2022.

Gallagher, M. E., Liljestrand, F. L., Hockaday, W. C., and Masiello, C. A.: Plant species, not climate, controls aboveground biomass O_2:CO_2 exchange ratios in deciduous and coniferous ecosystems, Journal of Geophysical Research: Biogeosciences, 122, 2314–2324, https://doi.org/10.1002/2017JG003847, 2017.

Hari, P., Nikinmaa, E., Pohja, T., Siivola, E., Bäck, J., Vesala, T., and Kulmala, M.: Station for measuring ecosystem-atmosphere relations: SMEAR, in: Physical and physiological forest ecology, pp. 471–487, Springer, 2013.

Hicks Pries, C., Angert, A., Castanha, C., Hilman, B., and Torn, M. S.: Using respiration quotients to track changing sources of soil respiration seasonally and with experimental warming, Biogeosciences, 17, 3045–3055, 2020.

Hilman, B., Weiner, T., Haran, T., Masiello, C. A., Gao, X., and Angert, A.: The apparent respiratory quotient of soils and tree stems and the processes that control it, Journal of Geophysical Research: Biogeosciences, 127, e2021JG006 676, 2022.

Ishidoya, S., Murayama, S., Takamura, C., Kondo, H., Saigusa, N., Goto, D., Morimoto, S., Aoki, N., Aoki, S., and Nakazawa, T.: O_2:CO_2 exchange ratios observed in a cool temperate deciduous forest ecosystem of central Japan , Tellus B: Chemical and Physical Meteorology, 65, 21 120, https://doi.org/10.3402/tellusb.v65i0.21120, 2013.

Ishidoya, S., Murayama, S., Kondo, H., Saigusa, N., Kishimoto-Mo, A. W., and Yamamoto, S.: Observation of O_2:CO_2 exchange ratio for net turbulent fluxes and its application to forest carbon cycles, Ecological Research, 30, 225–234, https://doi.org/10.1007/s11284-014-1241-3, 2015.

Jürgensen, J., Muhr, J., and Knohl, A.: Variations of the Oxidative Ratio across Ecosystem Components and Seasons in a Managed Temperate Beech Forest (Leinefelde, Germany), Forests, 12, 1693, 2021.

Keeling, R.: Development of an Interferometric Oxygen Analyzer for Precise Measurement of the Atmospheric O_2 Mole Fraction., Ph.D. thesis, Harvard University, 1988.

Keeling, R., Najjar, R., Bender, M., and Tans, P.: What atmospheric oxygen measurements can tell us about the global carbon-cycle, Global Biogeochemical Cycles, 7, 37–67, https://doi.org/10.1029/92GB02733, 1993.

Keeling, R. F. and Manning, A. C.: Studies of Recent Changes in Atmospheric O_2 Content, vol. 5, Elsevier Ltd., 2 edn., https://doi.org/10.1016/B978-0-08-095975-7.00420-4, 2014.

Keeling, R. F., Manning, A. C., McEvoy, E. M., and Shertz, S. R.: Methods for measuring changes in atmospheric O_2 concentration and their application in southern hemisphere air, Journal of Geophysical Research: Atmospheres, 103, 3381–3397, 1998.

Keeling, R. F., Manning, A. C., Paplawsky, W. J., and Cox, A. C.: On the long-term stability of reference gases for atmospheric O2/N2 and
CO$_2$ measurements, Tellus B: Chemical and Physical Meteorology, 59, 3–14, https://doi.org/10.1111/j.1600-0889.2006.00196.x, 2007.

Kljun, N., Calanca, P., Rotach, M., and Schmid, H. P.: A simple two-dimensional parameterisation for Flux Footprint Prediction (FFP),
Geoscientific Model Development, 8, 3695–3713, 2015.

Kohonen, K.-M., Dewar, R., Tramontana, G., Mauranen, A., Kolari, P., Kooijmans, L. M., Papale, D., Vesala, T., and Mammarella, I.:
Intercomparison of methods to estimate gross primary production based on CO 2 and COS flux measurements, Biogeosciences, 19,
4067–4088, 2022.

Kooijmans, L. M., Cho, A., Ma, J., Kaushik, A., Haynes, K. D., Baker, I., Luijkx, I. T., Groenink, M., Peters, W., Miller, J. B., et al.:
Evaluation of carbonyl sulfide biosphere exchange in the Simple Biosphere Model (SiB4), Biogeosciences, 18, 6547–6565, 2021.

Koren, G., Schneider, L., van der Velde, I. R., van Schaik, E., Gromov, S. S., Adnew, G. A., Mrozek Martino, D. J., Hofmann, M. E.,
Liang, M.-C., Mahata, S., et al.: Global 3-D Simulations of the Triple Oxygen Isotope Signature Δ17O in Atmospheric CO$_2$, Journal of
Geophysical Research: Atmospheres, 124, 8808–8836, 2019.

Korhonen, J., Pihlatie, M., Pumpanen, J., Aaltonen, H., Hari, P., Levula, J., Kieloaho, A.-J., Nikinmaa, E., Vesala, T., and Ilvesniemi, H.:
Nitrogen balance of a boreal Scots pine forest, Biogeosciences, 10, 1083–1095, 2013.

Kozlova, E. A. and Manning, A. C.: Methodology and calibration for continuous measurements of biogeochemical trace gas and O$_2$ con-
centrations from a 300-m tall tower in central Siberia, Atmospheric Measurement Techniques, 2, 205–220, https://doi.org/10.5194/amt-2-
205-2009, 2009.

Kulmala, L., Pumpanen, J., Kolari, P., Dengel, S., Berninger, F., Köster, K., Matkala, L., Vanhatalo, A., Vesala, T., and Bäck, J.: Inter-and
intra-annual dynamics of photosynthesis differ between forest floor vegetation and tree canopy in a subarctic Scots pine stand, Agricultural
and Forest Meteorology, 271, 1–11, 2019.

Manning, A. C.: Temporal variability of atmospheric oxygen from both continuous measurements and a flask sampling network: Tools for
studying the global carbon cycle, University of California, San Diego, 2001.

Manning, A. C. and Keeling, R. F.: Global oceanic and land biotic carbon sinks from the scripps atmospheric oxygen flask sampling network,
Tellus, Series B: Chemical and Physical Meteorology, 58, 95–116, https://doi.org/10.1111/j.1600-0889.2006.00175.x, 2006.

Mayer, J. C., Bargsten, A., Rummel, U., Meixner, F. X., and Foken, T.: Distributed Modified Bowen Ratio method
for surface layer fluxes of reactive and non-reactive trace gases, Agricultural and Forest Meteorology, 151, 655–668,
https://doi.org/10.1016/j.agrformet.2010.10.001, 2011.

Meyers, T. P., Hall, M. E., Lindberg, S. E., and Kim, K.: Use of the modified Bowen-ratio technique to measure fluxes of trace gases,
Atmospheric Environment, 30, 3321–3329, 1996.

Nguyen, L. N., Meijer, H. A., van Leeuwen, C., Kers, B. A., Scheeren, H. A., Jones, A. E., Brough, N., Barningham, T., Pickers, P. A.,
Manning, A. C., et al.: Two decades of flask observations of atmospheric δ (O$_2$/N$_2$), CO 2, and APO at stations Lutjewad (the Netherlands)
and Mace Head (Ireland), and 3 years from Halley station (Antarctica), Earth System Science Data, 14, 991–1014, 2022.

Paulson, C. A.: The mathematical representation of wind speed and temperature profiles in the unstable atmospheric surface layer, Journal
of Applied Meteorology and Climatology, 9, 857–861, 1970.

Peters, W., van der Velde, I. R., Van Schaik, E., Miller, J. B., Ciais, P., Duarte, H. F., van der Laan-Luijkx, I. T., van der Molen, M. K.,
Scholze, M., Schaefer, K., et al.: Increased water-use efficiency and reduced CO$_2$ uptake by plants during droughts at a continental scale,
Nature geoscience, 11, 744–748, 2018.

Peters, W., Bastos, A., Ciais, P., and Vermeulen, A.: A historical, geographical and ecological perspective on the 2018 European summer drought, Philosophical transactions of the royal society B, 375, 20190 505, 2020.

Physick, W. and Garratt, J.: Incorporation of a high-roughness lower boundary into a mesoscale model for studies of dry deposition over complex terrain, Boundary-Layer Meteorology, 74, 55–71, 1995.

940   Pickers, P. A., Manning, A. C., Sturges, W. T., Le Quéré, C., Mikaloff Fletcher, S. E., Wilson, P. A., and Etchells, A. J.: In situ measurements of atmospheric O_2 and CO_2 reveal an unexpected O_2 signal over the tropical Atlantic Ocean, Global Biogeochemical Cycles, 31, 1289–1305, 2017.

Pickers, P. A., Manning, A. C., Le Quéré, C., Forster, G. L., Luijkx, I. T., Gerbig, C., Fleming, L. S., and Sturges, W. T.: Novel quantification of regional fossil fuel CO_2 reductions during COVID-19 lockdowns using atmospheric oxygen measurements, Science advances, 8,

945   eabl9250, 2022.

Popa, M. E., Gloor, M., Manning, A. C., Jordan, A., Schultz, U., Haensel, F., Seifert, T., and Heimann, M.: Measurements of greenhouse gases and related tracers at Bialystok tall tower station in Poland, Atmospheric Measurement Techniques, 3, 407–427, https://doi.org/10.5194/amt-3-407-2010, 2010.

Randerson, J. T., Masiello, C. A., Still, C. J., Rahn, T., Poorter, H., and Field, C. B.: Is carbon within the global terrestrial biosphere be-

950   coming more oxidized? Implications for trends in atmospheric O_2 , Global Change Biology, 12, 260–271, https://doi.org/10.1111/j.1365-2486.2006.01099.x, 2006.

Reichstein, M., Falge, E., Baldocchi, D., Papale, D., Aubinet, M., Berbigier, P., Bernhofer, C., Buchmann, N., Gilmanov, T., Granier, A., et al.: On the separation of net ecosystem exchange into assimilation and ecosystem respiration: review and improved algorithm, Global change biology, 11, 1424–1439, 2005.

955   Rödenbeck, C., Le Quéré, C., Heimann, M., and Keeling, R. F.: Interannual variability in oceanic biogeochemical processes inferred by inversion of atmospheric O_2/N_2 and CO_2 data, Tellus, Series B: Chemical and Physical Meteorology, 60 B, 685–705, https://doi.org/10.1111/j.1600-0889.2008.00375.x, 2008.

Rousseeuw, P. J. and Verboven, S.: Robust estimation in very small samples, Computational Statistics & Data Analysis, 40, 741–758, 2002.

Seibt, U., Brand, W. A., Heimann, M., Lloyd, J., Severinghaus, J. P., and Wingate, L.: Observations of O_2 : CO_2 exchange ratios during

960   ecosystem gas exchange, Global Biogeochemical Cycles, 18, 1–18, https://doi.org/10.1029/2004GB002242, 2004.

Severinghaus, J. P.: Studies of the Terrestrial O_2 and Carbon Cycles in Sand Dune Gases and in Biosphere, Ph.D. thesis, Columbia University, https://doi.org/10.2172/477735, 1995.

Stephens, B. B., Keeling, R. F., Heimann, M., Six, K. D., Murnane, R., and Caldeira, K.: Testing global ocean carbon cycle models using measurements of atmospheric O_2 and CO_2 concentration, Global Biogeochemical Cycles, 12, 213–230, https://doi.org/10.1029/97GB03500,

965   1998.

Stephens, B. B., Bakwin, P. S., Tans, P. P., Teclaw, R. M., and Baumann, D. D.: Application of a differential fuel-cell analyzer for measuring atmospheric oxygen variations, Journal of Atmospheric and Oceanic Technology, 24, 82–94, https://doi.org/10.1175/JTECH1959.1, 2007.

Stull, R. B.: An introduction to boundary layer meteorology, vol. 13, Springer Science & Business Media, 1988.

Tohjima, Y., Machida, T., Watai, T., Akama, I., Amari, T., and Moriwaki, Y.: Preparation of gravimetric standards for measurements of at-

970   mospheric oxygen and reevaluation of atmospheric oxygen concentration., Journal of Geophysical Research–Atmospheres, 110, D11 302, https://doi.org/10.1029/2004JD005595, 2005.

Tohjima, Y., Mukai, H., Machida, T., Hoshina, Y., and Nakaoka, S.-I.: Global carbon budgets estimated from atmospheric $\delta O_2/N_2$ and CO_2 observations in the western Pacific region over a 15-year period, Atmospheric Chemistry and Physics, 19, 9269–9285, 2019.

van der Laan, S., van der Laan-Luijkx, I. T., Rödenbeck, C., Varlagin, A., Shironya, I., Neubert, R. E., Ramonet, M., and Meijer, H. A.: Atmospheric CO_2, $\delta(O_2/N_2)$, APO and oxidative ratios from aircraft flask samples over Fyodorovskoye, Western Russia, Atmospheric Environment, 97, 174–181, https://doi.org/10.1016/j.atmosenv.2014.08.022, 2014.

van der Laan-Luijkx, I. T., Neubert, R. E., van der Laan, S., and Meijer, H. A.: Continuous measurements of atmospheric oxygen and carbon dioxide on a North Sea gas platform, Atmospheric Measurement Techniques, 3, 113–125, https://doi.org/10.5194/amt-3-113-2010, 2010.

van Leeuwen, C. and Meijer, H. A.: Detection of CO_2 leaks from carbon capture and storage sites with combined atmospheric CO_2 and O_2 measurements, International Journal of Greenhouse Gas Control, 41, 194–209, https://doi.org/10.1016/j.ijggc.2015.07.019, 2015.

Vilà-Guerau de Arellano, J., Gioli, B., Miglietta, F., Jonker, H. J., Baltink, H. K., Hutjes, R. W., and Holtslag, A. A.: Entrainment process of carbon dioxide in the atmospheric boundary layer, Journal of Geophysical Research Atmospheres, 109, 1–16, https://doi.org/10.1029/2004JD004725, 2004.

Wehr, R., Munger, J., McManus, J., Nelson, D., Zahniser, M., Davidson, E., Wofsy, S., and Saleska, S.: Seasonality of temperate forest photosynthesis and daytime respiration, Nature, 534, 680–683, 2016.

Whelan, M. E., Lennartz, S. T., Gimeno, T. E., Wehr, R., Wohlfahrt, G., Wang, Y., Kooijmans, L. M. J., Hilton, T. W., Belviso, S., Peylin, P., Commane, R., Sun, W., Chen, H., Kuai, L., Mammarella, I., Maseyk, K., Berkelhammer, M., Li, K.-F., Yakir, D., Zumkehr, A., Katayama, Y., Ogée, J., Spielmann, F. M., Kitz, F., Rastogi, B., Kesselmeier, J., Marshall, J., Erkkilä, K.-M., Wingate, L., Meredith, L. K., He, W., Bunk, R., Launois, T., Vesala, T., Schmidt, J. A., Fichot, C. G., Seibt, U., Saleska, S., Saltzman, E. S., Montzka, S. A., Berry, J. A., and Campbell, J. E.: Reviews and syntheses: Carbonyl sulfide as a multi-scale tracer for carbon and water cycles, Biogeosciences, 15, 3625–3657, https://doi.org/10.5194/bg-15-3625-2018, 2018.

Wolf, A., Saliendra, N., Akshalov, K., Johnson, D. A., and Laca, E.: Effects of different eddy covariance correction schemes on energy balance closure and comparisons with the modified Bowen ratio system, Agricultural and Forest Meteorology, 148, 942–952, https://doi.org/10.1016/j.agrformet.2008.01.005, 2008.

Worrall, F., Clay, G. D., Masiello, C. A., and Mynheer, G.: Estimating the oxidative ratio of the global terrestrial biosphere carbon, Biogeochemistry, 115, 23–32, https://doi.org/10.1007/s10533-013-9877-6, 2013.